

See discussions, stats, and author profiles for this publication at: <https://www.researchgate.net/publication/378471537>

Carbon dioxide removal via weathering of sugarcane-mill ash under different soil conditions

Article in *Applied Geochemistry* · February 2024

DOI: [10.1016/j.apgeochem.2024.105940](https://doi.org/10.1016/j.apgeochem.2024.105940)

CITATIONS

7

READS

81

4 authors, including:



Hannah Green

James Cook University

5 PUBLICATIONS 16 CITATIONS

[SEE PROFILE](#)

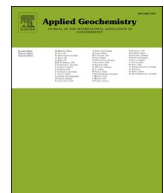


Paul N. Nelson

James Cook University

158 PUBLICATIONS 7,573 CITATIONS

[SEE PROFILE](#)



Carbon dioxide removal via weathering of sugarcane mill ash under different soil conditions

Hannah Green ^{a,*}, Peter Larsen ^b, Yang Liu ^a, Paul N. Nelson ^c

^a James Cook University, 1 James Cook Dr, Douglas, Townsville, Queensland, 4811, Australia

^b Wilmar Sugar Australia Pty Ltd, 5-21 Denham Street, Townsville, Queensland, 4810, Australia

^c James Cook University, McGregor Road, Smithfield, Cairns, Queensland, 4878, Australia

ARTICLE INFO

Editorial handling by: Dr. Tao Wen

Keywords:

Basalt
Carbon sequestration
Enhanced weathering
Industrial by-product
Soil chemistry
Geochemical modelling
Negative-emission technology

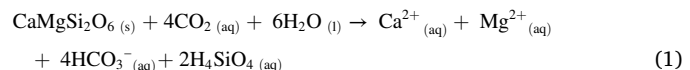
ABSTRACT

Sugarcane mill ash has been suggested as having high potential for carbon dioxide removal (CDR) via enhanced weathering (EW), but this had not been quantitatively assessed. The aims of this study were to 1) assess the CDR potential of various sugarcane mill ashes via EW, and 2) investigate the impact of soil conditions and mill ash properties on the CDR. This was done by characterising physical and chemical properties of five mill ashes from Australia and simulating weathering using a one-dimensional reactive transport model. The model was parameterised to simulate weathering of 100 t/ha of wet ash (47–65% water) or crushed basalt for 15 years under various combinations of soil pH and carbon dioxide partial pressure ($p\text{CO}_2$). A sensitivity analysis was undertaken in a two-level factorial design to test the effect of pH, pH buffering, material surface area, infiltration rate, plant uptake of nutrients, organic matter cation exchange surfaces, and $p\text{CO}_2$ on modelled CDR. The simulated CDR of the mill ashes was significantly less than the basalt ($p < 0.001$) but mostly did not differ significantly between ashes ($p > 0.05$). Weathering of mill ash removed 0.0–4.0 t CO_2/ha (0.00–0.040 t CO_2/t wet ash) cumulatively, similar to some basalts and olivine modelled in the literature. The theoretical maximum CDR of the mill ashes (based on amount of weatherable material applied) was achieved in around 5 years. The estimate of CDR varied by orders of magnitude depending on conditions. It was least when initial soil solution pH was lowest (4.5, unbuffered), pH was at 6.5 or less with constant buffering, and $p\text{CO}_2$ was low (600 ppm). CDR was also significantly lower when calculated directly from accumulation of carbon in dissolved and solid phases rather than stoichiometrically from cation release. The effects of pH and pH buffering quantified here may explain low measured CDR from EW in field trials on acidic soils and highlight the need for more realistic modelling of pH buffering capacity. Overall, mill ash shows high potential for CDR via EW, especially if lifecycle benefits are considered, although this must be validated in the field.

1. Introduction

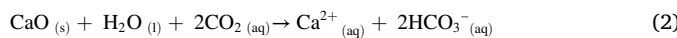
To limit future global warming to 1.5–2.0 °C, rapid reductions in greenhouse gas (GHG) emissions as well as widespread deployment of negative emissions technologies (NETs) are required (Gasser et al., 2015). NETs capture atmospheric carbon and sequester it in more-or-less permanent terrestrial or oceanic sinks (Hepburn et al., 2019). If emissions reduction targets are not met, reliance on NETs to prevent catastrophic global warming will become even greater. Additionally, the later NETs are engaged on a mass scale, the greater the risk of long-term environmental damage (Fuss et al., 2018; Obersteiner et al., 2018).

Enhanced weathering (EW) is a NET with promising carbon dioxide removal (CDR) potential (Schuiling and Krijgsman, 2006). It involves the weathering of calcium or magnesium silicates or oxides, during which gaseous carbon dioxide is converted to dissolved or precipitated carbonates. In the presence of water, carbon dioxide dissolves to form carbonic acid, which in turn produces bicarbonate and/or carbonate when it reacts with calcium or magnesium silicates or oxides via the following weathering reactions:



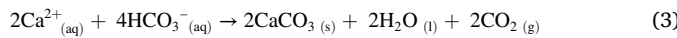
* Corresponding author. 1 James Cook Dr, Douglas, Townsville, Queensland, 4811, Australia.

E-mail addresses: hannah.green@my.jcu.edu.au (H. Green), peter.larsen@au.wilmar-intl.com (P. Larsen), yang.liu11@jcu.edu.au (Y. Liu), paul.nelson@jcu.edu.au (P.N. Nelson).



The dissolution of silicate minerals is common in nature but slow, whereas the high reactivity of calcium and magnesium oxides means they are uncommon in nature but can be found in industrial wastes such as ashes, slags, and cement. Weathering rate can be enhanced by increasing acidity (including carbonic acid), temperature, biological activity (especially plants and microorganisms), and mineral surface area (achieved by crushing in the case of rocks). Ideal conditions for weathering occur naturally in warm moist vegetated soils. Soils have high carbon dioxide concentrations (in the order of 2,000–24,000 ppm) due to respiration of plant roots, microorganisms, and fauna, which increases with temperature, moisture content, and inputs of organic matter (Amundson and Davidson, 1990; Connor, 2012; Luo and Zhou, 2006; Nan et al., 2016; Rastogi et al., 2002). As such, soils could potentially be large-scale carbon sinks via EW, especially in the tropics (Andrews and Taylor, 2019; Baek et al., 2023; Edwards et al., 2017; Hartmann et al., 2013; Kantola et al., 2017). Furthermore, soils under agriculture are ideal due to large areas of accessible land as well as the infrastructure to distribute weatherable material. Increased agricultural productivity has also been documented following application of calcium- and magnesium-rich silicate rocks and alkaline industrial wastes (e.g., Berthelsen et al., 2001; d'Hotman and de Villiers, 1961; Kingston, 1999; van Straaten, 2006), highlighting the potential for EW to improve food security and mitigate climate change simultaneously. However, the effects of different crops and crop management on CDR must be taken into account (Taylor et al., 2017; Amann and Hartmann, 2019; Beerling et al., 2018; Pratt et al., 2020; Swoboda et al., 2022; Zhang et al., 2018).

As weathering occurs, dissolved carbonates (principally bicarbonate) and cations are expected to accumulate in the soil or be transported through the soil profile to groundwater, streams, and eventually the ocean where storage is considered permanent in terms of climate change mitigation. Storage of dissolved bicarbonate sequesters twice as much carbon dioxide as precipitated carbonates due to precipitation releasing carbon dioxide (Equation (3)). Carbonate precipitation in soil and ocean environments depends primarily on temperature, pH, partial pressure of carbon dioxide, and concentration of calcium or magnesium cations (Renforth and Henderson, 2017; Zamanian et al., 2016).



Rocks and minerals commonly investigated for EW include olivine, basalt, and wollastonite due to their high weatherability and content of calcium and magnesium (Swoboda et al., 2022). The CDR potential of these materials have been assessed mostly via geochemical models and column/mesocosm experiments and shows promising but highly variable results. Potential CDR of these materials, calculated as R_{CO_2} (Equation (4)) ranged from 0.13 to 0.97 t CO₂/t material, and estimated CDR following application to land ranged over several orders of magnitude across studies (0.00–0.17 t CO₂/t material; Amann et al., 2020; Buckingham et al., 2022; Cipolla et al., 2021; Lefebvre et al., 2019; Lewis et al., 2021; Rinder and von Hagke, 2021). Variations between studies are at least partially due to differences in soil conditions or the way they were modelled. Concerns over the use of these materials for CDR include potential for heavy metal contamination, the requirement for additional mining, and the overall carbon and energy balance, including the requirement for comminution (crushing to increase surface area), transport, and spreading (Dupla et al., 2023; Smith et al., 2016a, 2016b).

Alkaline industrial wastes such as mineral processing slags, concrete, and ashes have been suggested as alternative feedstock for EW (Bobicki et al., 2012; Renforth, 2019). The CDR potential of these materials is highly variable ($R_{\text{CO}_2} = 0.03\text{--}0.78$ t CO₂/t material) and some would pose unacceptable contamination risk. However, their benefits over silicate rocks include no requirement for mining, recycling of existing waste products, potentially high surface area without the need for

additional comminution, and lower transport distances. Critically, although the CDR potential of various industrial wastes have been assessed, there is no study assessing the use of industrial wastes in an agricultural context.

Mill ash is a by-product of the sugarcane milling process. It is produced when bagasse (fibrous residue from crushing and extraction of juice from cane stalks) is combusted in boilers to generate steam for the milling process and is used to generate electricity for the mill and in some cases the broader grid. Approximately 4 million t/year of sugarcane mill ash is produced globally (Khalil et al., 2021) with the majority (around 2.7 million t/year) produced in Brazil (Frías et al., 2011). Around 200, 000 t/year is produced by the Australia sugar industry (Moody et al., 2014). As a means of disposal, it often accumulates in landfill or it is commonly applied to soils within 20 km of the mill at rates up to 300 t/ha (Frías et al., 2011; Queensland Department of Environment and Science, 2022). It has high water content because it is washed from the boilers. Mill ash is known to have nitrogen (if combustion is incomplete), phosphorus, potassium, and silicon nutrient value as well as liming value (see Table S1; Barry et al., 1998; Barry et al., 2001; Berthelsen et al., 2001; Moody et al., 2014; Khalil et al., 2021) and has been shown to increase sugarcane productivity (Berthelsen et al., 2001; Kingston, 1999; Larsen et al., 2023).

Due to its high base cation and silica content, it has been suggested that mill ash has high potential for CDR via EW (Beerling et al., 2018), although a proper assessment has yet to be undertaken. Increases in soil pH have been measured after application of mill ash, indicating the generation of bicarbonate and carbonate from weathering (Barry et al., 2001; Marchuk et al., 2018; Moody et al., 2014; Nguyen et al., 2014; Stirling et al., 2018), but no study has attempted to quantify CDR via weathering of mill ash. Mill ash is only applied to a limited area so the location (based on soil type, climate, and transport distance) and application rate could be optimised for CDR, if it can be demonstrated. This could partially offset carbon emissions associated with sugar production, increase the value of this waste product, and improve the management and redistribution of nutrients. Furthermore, mill ash has other potential uses, such as pozzolan for cement (Frías et al., 2011), so knowing its CDR value will facilitate comparison of alternative uses.

Field studies to quantify CDR via EW must be carried out before EW is deployed at large scales, but geochemical modelling studies are also crucial. Quantitative modelling enables better understanding of the processes and their interactions, especially if sensitivity analyses are conducted. That understanding facilitates design of field experiments to examine key unknowns. Furthermore, when calibrated with measured data, modelling allows extrapolation to scenarios (e.g., climate, soil, vegetation, management) and time scales that are not feasible to examine experimentally. Finally, adequate monitoring, reporting and verification (MRV) of CDR via EW in commercial projects will not be feasible via measurements in the field, so it will rely on development of sufficiently accurate geochemical models. To address the unknowns described above, the aims of this study were to.

1. Assess the CDR potential of various sugarcane mill ashes via EW using a one-dimensional reactive transport model, relative to a previously studied basalt.
2. Investigate the impacts of material surface area, soil pH, soil pH buffering, infiltration rate (or transport time step duration), plant uptake of nutrients, organic matter cation exchange capacity, and partial pressure of carbon dioxide on modelled CDR via EW of mill ash and basalt.

2. Materials and methods

2.1. Collection of mill ash for characterisation and model parameterisation

Moisture content and chemical composition of sugarcane mill ash

varies over space and time, so samples were collected from five mills in North Queensland in March–August 2022 to capture this variability. Samples of sugarcane mill ash were collected from Racecourse Mill in Mackay, Victoria Mill in Ingham, Pioneer Mill in Ayr, Tablelands Mill near Mareeba, and Mulgrave Mill in Gordonvale. A sample of bagasse was collected from Racecourse Mill. Samples were randomly collected from recently produced stockpiles, oven-dried at 70 °C until constant weight, and then stored at room temperature. Water content of the dried materials was analysed gravimetrically by heating subsamples to 105 °C until constant weight, and all analytical results are expressed on an oven-dry equivalent basis. All chemical analyses were conducted at the Advanced Analytical Centre and Analytical Chemistry laboratory at James Cook University.

2.2. Chemical analysis of mill ash

The total elemental composition of the inorganic components of each material were measured via inductively coupled plasma atomic emission spectrometry (ICP-AES) of an acid digest, and X-ray fluorescence (XRF; Table 1). All samples were heated to 1000 °C in a furnace and the change in mass before and after heating was recorded as loss on ignition (LOI). Samples were then fused with 12:22 lithium borate flux. The resulting fused glass bead was semi-quantitatively analysed via XRF using a Bruker-AXS S4 Pioneer X-ray Fluorescence Spectrometer and SpectraPlus software. For ICP-AES analysis, the fused beads were crushed, 0.5 g was dissolved in 10% HNO₃ to make up 50 mL, and this was diluted 5-fold. Triplicate samples were analysed using a Varian Liberty Series II ICP-AES.

The theoretical maximum CDR potential ($t \text{ CO}_2/t \text{ material}$; R_{CO_2}) of the dry mill ashes was calculated using the ICP-AES and XRF elemental compositions according to Renforth (2012):

$$R_{CO_2} = \frac{M_{CO_2}}{100} \times \left(2 \times \left(\frac{\%_{Ca}}{M_{Ca}} + \frac{\%_{Mg}}{M_{Mg}} \right) + \left(\frac{\%_{Na}}{M_{Na}} + \frac{\%_K}{M_K} \right) \right) \quad (4)$$

where M is the molar mass of each species. The constant commonly used in R_{CO_2} and CDR calculations to account for the reduction in CDR efficiency when cations are transported to the ocean was excluded. This is because of spatial and temporal variability and unknowns regarding downstream losses (Kanzaki et al., 2023). Additionally, this paper focuses on the effects of soil chemistry on CDR via EW rather than downstream processes.

Carbon content and nitrogen was measured using a Costech elemental analyser (EA) with thermal conductivity detector (Table 2). For total carbon and nitrogen, samples were introduced directly. For total organic carbon, samples were pretreated by immersion in 2 M HCl for 3 h. For charcoal carbon (or stable polyaromatic carbon, pyrogenic carbon, black carbon, or in this case, soot), samples were pretreated by hydrogen pyrolysis (Ascough et al., 2009). Approximately 250 mg of each sample was mixed with a molybdenum catalyst using an aqueous methanol solution of ammonium dioxydithiomolybdate, sonicated, and dried at 60 °C. The mixture was placed in a reactor, pressurized with H₂ to 150 bar with a purge gas flow of 5 L/min and heated at 300 °C/min to 250 °C, then at 8 °C/min to 550 °C, where it was held for 5 min. Inorganic carbon content was determined using thermogravimetric analysis (TGA). This was done using a STD 650 Thermal Analyser with TA Instruments Trios software (version 4.2.1.36612). Around 20 g of sample was placed in 90 µL ceramic crucibles and heated at 50 °C/min from room temperature (25 °C) to 500 °C, then at 10 °C/min to 1000 °C, where it was held for 10 min. Flow of nitrogen (N₂) gas at 50 mL/min was maintained during the temperature ramping. Carbonate content was determined as the mass loss between 500 and 900 °C (Bensharada et al., 2022; Kristl et al., 2016).

Mineralogy was determined using X-ray diffraction (XRD) using a Bruker D2 Phaser 2nd Gen diffractometer (Table 3). Samples were pressed into mounting discs and scanned from 5 to 85 °2θ at 67 °2θ/minute. Crystalline phases were identified by Siroquant using Siroquant V4 Rietveld software. The content of amorphous material (including crystalline material below the detection limit of 2%) was determined via mass balance. The elemental composition of the amorphous material was determined by subtracting the elemental composition of the identified crystalline materials plus carbon containing species from the total elemental composition determined by acid digestion-ICP-AES and XRF. Two scenarios were calculated using the highest and lowest estimates across both methods. The materials comprising the unaccounted-for elements were assumed based on materials identified in previous work on sugarcane mill ash (Clark et al., 2017; Jordan and Akay, 2012) and other biomass ashes (Vassilev et al., 2013). Unaccounted-for silicon was assumed to be present as amorphous silica (SiO_2), phosphorus as calcium and magnesium phosphates ($\text{Ca}_3(\text{PO}_4)_2$ and $\text{Mg}_3(\text{PO}_4)_2$), and aluminium, iron, potassium, and titanium as oxides (Al_2O_3 , Fe_2O_3 , K_2O , and TiO_2). Remaining calcium and magnesium were assumed to be present as calcium and magnesium hydroxide ($\text{Ca}(\text{OH})_2$ and $\text{Mg}(\text{OH})_2$)

Table 1

Elemental composition of samples based on ICP-AES and XRF. All elements and loss on ignition (LOI) values are given as a proportion of the original dry mass (%) and water is given as a proportion of original wet mass (%). R_{CO_2} values are in t CO₂/t dry material.

Table 2

Total carbon, charcoal carbon, non-charcoal organic carbon, inorganic (carbonate) carbon, and total nitrogen in each sample as a proportion of dry mass (%). The detection limit for total nitrogen was 0.02%. Results shown are the mean of three replicates. Some values were excluded as outliers, so the sum of charcoal carbon, non-charcoal organic carbon, and inorganic carbon does not equal total carbon in every case.

Component containing C/N	Racecourse bagasse	Racecourse mill ash	Victoria mill ash	Pioneer mill ash	Tablelands mill ash	Mulgrave mill ash
Total C	40.4	2.40	5.50	4.29	2.47	2.26
Charcoal C	–	2.30	5.39	3.45	2.06	2.09
Non-charcoal organic C	–	0.00	0.00	0.59	0.21	0.00
Inorganic C	–	0.24	0.19	0.26	0.19	0.00
Total N	0.20	<0.02	0.06	0.04	<0.02	0.03

Table 3

Mineralogy and amorphous material composition of mill ash samples based on XRD, TGA, and mass balance. Phases are given as proportion of the original dry mass. For XRD traces see Fig. S3. The detection limit for total nitrogen was 2%.

Phase	Formula	Racecourse	Victoria	Pioneer	Tablelands	Mulgrave
<i>Amorphous content</i>		46	58	72	46	40
Silica	SiO ₂	24.6	35.6	41.0	22.0	18.6
Aluminium oxide	Al ₂ O ₃	3.7	3.0	7.6	6.8	6.4
Iron oxide	Fe ₂ O ₃	3.8	1.2	3.2	4.2	2.6
Charcoal	C	2.3	5.4	3.5	2.1	2.4
Potassium oxide	K ₂ O	0.0	1.6	1.7	1.1	2.0
Magnesium hydroxide	Mg(OH) ₂	2.0	1.2	1.7	2.0	1.4
Calcium carbonate	CaCO ₃	1.3	1.6	2.2	1.6	0.0
Calcium phosphate	Ca ₃ (PO ₄) ₂	0.9	0.6	0.5	1.0	0.4
Magnesium phosphate	Mg ₃ (PO ₄) ₂	0.7	0.5	0.5	0.8	0.3
Calcium hydroxide	Ca(OH) ₂	1.2	0.5	0.0	0.3	0.7
Titanium oxide	TiO ₂	0.6	0.3	0.6	0.6	0.5
Manganese oxide	MnO ₂	0.3	0.2	0.2	0.4	0.2
Organic matter		0.0	0.0	1.2	0.4	0.0
<i>Crystalline content</i>		54	44	27	54	60
Quartz	SiO ₂	35	22	19	34	57
Potassium Feldspar	KSi ₃ AlO ₈	11	12	3	10	1
Plagioclase Feldspar	NaSi ₃ AlO ₈	3	8	5	8	2
Illite/Muscovite	KAl ₂ (Si ₃ Al)O ₁₀ (OH,F) ₂	5	<2	<2	2	Possible
Vivianite	(Fe,Mg,Mn) ₃ (PO ₄) ₂ ·8H ₂ O	Possible	<2	<2	Possible	<2

rather than oxides due to their high reactivity with water (see Table 3).

The particle morphology (shape, size, surface texture) of the Tablelands and Racecourse ash samples was assessed using scanning electron microscopy (SEM; Fig. S1). Samples were stub-mounted and coated in platinum to approximately 10 nm thick. Samples were then viewed using a Jeol JSM 5410LV SEM. Lower magnification images were acquired with the SEM operating at an accelerating voltage of 20,000 V under high vacuum conditions and higher magnification images were acquired with the SEM operating at an accelerating voltage of 3000 V under low vacuum conditions. Additionally, the elemental composition of particles at specific points was identified and semi-quantitatively measured using a Jeol JXA 8200 SuperProbe fitted with an energy dispersive spectrometer. The detection limit for most elements was between 0.02 and 0.6 wt %.

2.3. Particle size and surface area analysis

Around 20-g sub-samples of each ash were sieved through 75, 125, 150, 250, 500, 1000, 2000, and 4000 µm sieves using an Endecotts Octagon Digital sieve shaker for 6 min. The amount of sample on each sieve was weighed and the proportion in each size fraction calculated. The particle size distribution of the <75 µm fraction was determined using a Mastersizer 3000 laser particle size analyser and Malvern software (version 3.81). Dry samples were dispersed in a beaker of de-ionised water sat inside a Soniclean 500 TD Digital Ultrasonic Cleaner for 2 min. The suspended samples were gradually added to the beaker of de-ionised water attached to the laser particle size analyser until an obscuration rate of 10–15% was achieved. Samples were then sonicated for 30 s before triplicate measurements were made.

Specific surface area (SSA) of the samples was measured by nitrogen (N₂) adsorption using the BET method (Brunauer et al., 1938).

Sub-samples of around 1.0 g were placed into measurement tubes and degassed overnight at 60 °C to remove gas and water using a Quantachrome Autosorb iQ. Samples were weighed after degassing and the weights were used in surface area calculations conducted in Quantachrome ASiQwin Automated Gas Sorption Data Acquisition and Reduction software (version 5.2). The samples were run on a 7-adsorption pressure point program from 0.1 to 2.5 P/P₀. Geometric SSA was also calculated using the results of the mass fraction sieving according to Kelland et al. (2020; Supplementary Information). Roughness ratio was calculated as BET SSA divided by geometric SSA.

2.4. Reactive transport modelling

To assess the CDR potential of the mill ashes, the one-dimensional reactive transport model (RTM) of Kelland et al. (2020), also used by Lewis et al. (2021), was employed to simulate weathering (see Data Availability for code). The model simulates the mass transfer of cations and alkalinity from the constituent minerals and amorphous material to aqueous solution over 15 years. A soil profile 0.5 m deep was simulated using ten 0.05-m deep cells with the equivalent of 100 t/ha of basalt or wet mill ash (to reflect the way it is applied in the field) incorporated into the upper 0.25 m. At each time step, fresh soil solution entered at the top of the first cell and soil solution from each cell was transported to the one immediately below as per Kelland et al. (2020). Within each timestep, kinetic reactions were solved using the Runge-Kutta method of solving ordinary differential equations. Unless specified, model parameters were the same as those used by Lewis et al. (2021). The basalt used was the Tichum Creek basalt studied by Lewis et al. (2021) and the model was parameterised as to produce the same CDR as reported by Lewis et al. (2021) under the same conditions. The model was run in PHREEQC (Linux batch version 3.7.3; Parkhurst and Appelo, 2013) on

the James Cook University high performance research computing cluster using the Amm.T-H.dat geochemical reaction database employed by Lewis et al. (2021). The model outputs were read into R (version 4.3.1; R Core Team, 2023) to calculate CDR. Results were visualised using the package ggplot2 (Wickham, 2016).

Several adjustments were made to the original model to represent tropical soil conditions, and scenarios were run at different levels of pH and carbon dioxide partial pressure ($p\text{CO}_2$). The infiltration rate was increased to 1000 mm/year to reflect higher deep drainage rates in sugarcane growing regions, and transport parameters were adjusted accordingly. As such, the transport time step duration was set to 3.7 days. Scenarios were run with initial soil solution pH at 4.5, 5.5, and 6.5, which covers the typical range occurring in tropical agricultural soils (Bruce et al., 1989). The model does not incorporate pH buffering reactions that occur in soil, which was reflected in unrealistically high levels of pH being reached in some of the simulations. Therefore, as well as being run as is ('unbuffered'), the model was also run with pH buffered at a constant level ('constantly buffered') through the addition of a conjugate acid-base pair (HNO_3 and NO_3^-). This was modelled as pseudo equilibrium phases according to Example 8 of the PHREEQC documentation (Parkhurst and Appelo, 2013). Although both unrealistic extremes, the unbuffered and constantly buffered scenarios were considered to bracket the range of soil pH buffering capacities likely to occur and demonstrate the effect of pH on CDR via EW. At each level of soil solution pH, scenarios were run with $p\text{CO}_2$ set at low (600 ppm throughout profile), high (12,000 ppm in top cell to 24,750 ppm in bottom cell) or moderate level (see Table S2 for details). Note that seasonal variation in $p\text{CO}_2$ is often large but is outside of the scope of this model.

For the modelling, mineral contents of the ash were based on XRD measurements, except calcite content, which was based on TGA carbonate measurements (Table 3). The content of amorphous material was based on the mass balance. The composition of the Tichum Creek basalt was based on data of Lewis et al. (2021, Table S2). The dissolution rate of minerals and amorphous materials (excluding basaltic glass) was modelled as a function of their surface area, temperature, and soil solution pH. This followed the irreversible equation described by Palandri and Kharaka (2004):

$$\frac{dm}{dt} = -SA \cdot \left[A_{acid} e^{\frac{-E_{acid}}{RT}} \cdot a_{H+}^{n_{acid}} \cdot (1 - SR) + A_{neutral} e^{\frac{-E_{neutral}}{RT}} \cdot (1 - SR) + A_{base} e^{\frac{-E_{base}}{RT}} \cdot a_{H+}^{n_{base}} \cdot (1 - SR) \right] \quad (5)$$

where m is the number of moles of the mineral, t is time (s), SA is the surface area (m^2), A is the pre-exponential factor (the rate constant, $\text{mol}/\text{m}^2/\text{s}$), E is the activation energy (J/mol), T is the temperature (K), R is the gas constant for water (8.31, J/mol/K), a is the ion activity of hydrogen (H^+), SR is the saturation ratio, and n is the reaction order for the acid, neutral, and base dissolution mechanism.

The surface area of each mineral and amorphous material was assigned as a proportion of the total surface area of the ash or basalt according to BET measurements based on their relative abundances. The rate constants, activation energies, and reaction orders for each mineral were extracted from Palandri and Kharaka (2004). Where values were not available, substitutions using similar minerals were made if possible and some minor phases were excluded from the model (Table S3). In line with Kelland et al. (2020) and Lewis et al. (2021), weathering of basaltic glass was modelled using the equation and rate constants of Flaathen et al. (2010). Due to a lack of data, weathering of amorphous silica was modelled using the same parameters. Saturation ratios were calculated using equilibrium constants from the THERMODDEM database (version 1.15; Blanc et al., 2012) and standard PHREEQC databases (phreeqc.dat and Tipping_Hurley.dat; Appelo and Postma, 2005; Table S4). In the case of amorphous silica, equilibrium constants were extracted from

Blecker et al. (2006) and those for basaltic glass were taken from Aradóttir et al. (2012).

As per Kelland et al. (2020), elements released by weathering were transported down the profile or taken up by one of three biogeochemical sinks. The first of these sinks was reversible sorption to solid phases modelled as cation exchange capacity (CEC) on clays, organic matter, and hydrous ferric oxide. The second sink was the reversible precipitation-dissolution of secondary mineral phases: aluminium hydroxide (Al(OH)_3), silica (SiO_2), and iron hydroxide (Fe(OH)_3). Calcite was also treated as a reversible phase in equilibrium with soil solution. The final sink was plant uptake of calcium, magnesium, and potassium by a sugarcane crop 120 days each year (adapted from sorghum in the original model). For mill ash models, additional plant uptake was determined based on sugarcane yield figures and rates of residue removal from the field (Mitchell and Larsen, 2000; Wilmar Sugar; Mitchell et al., 2000). Additional plant uptake was not included in the basalt models as no sugarcane yield response has been recorded in the field (unpublished data from a current field trial).

Carbon dioxide removal was calculated in two ways, one being that used by Lewis et al. (2021) and others, based stoichiometrically on production of cations during weathering, assuming carbonic acid weathering ($\text{CDR}_{\text{cations}}$), and the other being from the sum of bicarbonate and carbonate produced in the soil environment ($\text{CDR}_{\text{carbon}}$). For every 1 mol of charge of cations (calcium, magnesium, sodium, and potassium) transferred to solution via weathering by carbonic acid, 1 mol of carbon dioxide is converted to bicarbonate (Equations (1) and (2)). As such, $\text{CDR}_{\text{cations}}$ (in t CO_2/ha) was calculated as the cumulative sum of cations in soil solution transported to the bottom of the soil profile (outflow from the tenth cell) at each time step over 15 years:

$$\text{CDR}_{\text{cations}} = \Delta \left[2 \times \sum ([\text{Ca}^{2+}] + [\text{Mg}^{2+}]) + \sum ([\text{Na}^+] + [\text{K}^+]) \right] \times W \times L \times M_{\text{CO}_2} \div 1,000,000 \quad (6)$$

where concentrations of cations are direct outputs of PHREEQC (moles/L of water), W is volumetric water content of each cell (0.2 m/m), L is the volume of each cell over 1 ha (500,000 L/ha), and M_{CO_2} is the molar mass of carbon dioxide. The Δ reflects the fact that "blank" models were also run, excluding all mineral saturation and weathering sections of code. This was to establish the background rate of ion production/consumption, which was subsequently subtracted at each time step to calculate the effect of weathering. $\text{CDR}_{\text{carbon}}$ was also calculated as the cumulative sum of bicarbonate generated and transported in the soil solution to the bottom of the profile at each time step over 15 years:

$$\text{CDR}_{\text{carbon}} = \Delta \left[\sum [\text{HCO}_3^-] \right] \times W \times L \times M_{\text{CO}_2} \div 1,000,000 \quad (7)$$

The amount of carbonate precipitated throughout the entire soil profile was also calculated but was zero under all scenarios except for basalt at low $p\text{CO}_2$ and high initial soil solution pH (Table S5; Fig. S2) so it is not included in Equation (7).

Generalised linear modelling (GLM) was performed to determine the effects of material, initial soil solution pH, pH buffering, and $p\text{CO}_2$ on cumulative CDR after 15 years. Analyses were completed using the glm function from the stats package (R Core Team, 2021) and glmmTMB function from the glmmTMB package (Brooks et al., 2017). Models were validated using DHARMA residuals (Hartig, 2022) and all defined contrasts were orthogonal. The best model for the number of parameters was determined using the corrected Akaike Information Criterion (AICc; Akaike, 1973).

2.5. Sensitivity analysis

A sensitivity analysis was performed to explore the impact of various parameters on the model estimates of CDR potential. This was done using a 2^k factorial design in which each parameter had two levels (high and low), and all possible combinations of parameters were tested

(Saltelli and Annoni, 2010). Although this design does not explore the full extent of each parameter space, it allows for all main and interaction effects to be tested and does not assume model linearity like other sensitivity analysis designs. The size of the main effects plus those of some key interactions were calculated as the difference in cumulative CDR after 15 years between the high and low scenarios, according to Saltelli and Annoni (2010). Mineralogical composition was kept constant to reflect the Tablelands mill ash. Parameters tested were chosen based on their expected impact on the model output and included organic carbon cation exchange sites, initial pH, presence/absence of pH buffering (at initial soil solution pH of 5.5), material surface area, pCO_2 , presence/absence of plant uptake of nutrients, and infiltration rate i.e., transport time step duration (Table S6). Multiple pH buffered models produced incongruous results at a few single time steps i.e., values for all model outputs were extremely high or low, returning to the previous levels in the next time step. This was identified as a vertical increase in the cumulative CDR over time curves followed by a return to the expected trajectory. These time steps were identified and removed from the output files before further analysis.

3. Results

3.1. Chemical and physical properties of mill ash

The ratios of major elements i.e., Si, Al, Fe, K, Ca, Mg, Na, and P, to each other in the bagasse were within the same range as in the mill ashes (Table 1). This indicates that all these elements are retained to the same extent during combustion. On average, over half the mass of the mill ashes was composed of amorphous material, and less than half was identifiable crystalline material (Table 3). All mill ashes had similar mineralogy, with quartz being the most common mineral and silica being the most common amorphous material. There was a similar proportion of silicon in each mill ash (30.56–35.34%; Table 1), however, mill ashes differed in the proportion of silicon present in crystalline/amorphous form (Table 3). At least some of the amorphous silica present was melted material (Fig. S1).

Carbon content was low in all mill ashes (<5.50% dry weight; Table 2). Organic carbon was below detection limit in most mill ashes and <0.60% in all, but some unburnt fragments were observed (Fig. S1). All mill ashes except Mulgrave contained a small amount of inorganic carbon, i.e., carbonate (Table 2), similar to the concentration in Tichum Creek basalt (0.22%; Lewis et al., 2021).

The mill ashes had BET SSA ranging from 20.5 to 51.0 m^2/g , with most being ~30 m^2/g (Table 4). These values were two to five times higher than commercial ‘crusher dust’ sample of Tichum Creek basalt (10.3 m^2/g ; Lewis et al., 2021). Most mill ash particles were <100 μm in diameter (Fig. S4).

3.2. Carbon dioxide removal values

Theoretical maximum CDR potential (R_{CO_2} values, based on ICP-AES measurements), ranged from 0.052 to 0.104 t CO_2/t dry mill ash for the Mulgrave and Racecourse mill ashes, respectively (Table 1). Those values represent 17–34% of the Tichum Creek basalt R_{CO_2} (0.31 t CO_2/t material). The ranking of materials in terms of R_{CO_2} values was the same

Table 4

Specific surface area (SSA; m^2/g) of each mill ash sample measured by BET isotherm and particle size distribution (geometric). Surface roughness is the ratio of BET to geometric SSA.

Surface property	Racecourse	Victoria	Pioneer	Tablelands	Mulgrave
BET SSA	30.1	31.7	51.0	31.7	20.5
Geometric SSA	13.0	11.8	11.3	13.2	11.0
Surface roughness	2.3	2.7	4.5	2.4	1.9

as their ranking for cumulative $CDR_{cations}$ and CDR_{carbon} values after 15 years (Table 5). Of the mill ashes, Mulgrave had the lowest CDR and Racecourse the highest. In terms of the proportion of maximum potential CDR reached, the materials were ranked in opposite order, with Mulgrave reaching up to 99% of the potential when initial soil solution pH was 6.5 and unbuffered and pCO_2 was high.

Variation in $CDR_{cations}$ was explained best (lowest AICc model that met assumptions) by material type only (Gamma distribution with log link). There was a significant difference between the cumulative CDR of the Tichum Creek basalt and all of the mill ashes ($p < 0.001$). There was no significant difference between each of the mill ashes ($p > 0.05$) except between the $CDR_{cations}$ of Racecourse and Mulgrave and Victoria and Mulgrave ($p < 0.05$). Rerelease of carbon dioxide via precipitation of calcite (Equation (3)) only occurred with Tichum Creek basalt. This reduced the overall CDR of the Tichum Creek basalt by up to 3.5 t CO_2/ha under the low pCO_2 and high initial soil solution pH scenario (Table S5; Fig. S2). The mill ashes generally achieved a higher proportion of their maximum potential CDR than the Tichum Creek basalt (Tables 5 and 6). Cumulative CDR of the mill ashes near plateaued after approximately five years while cumulative CDR of the Tichum Creek basalt did not plateau within the 15 year timeframe modelled (Figs. 1 and 2). Across materials, there was a clear trend of increasing CDR with pCO_2 and initial soil solution pH (Figs. 1 and 2). At high values of those two variables, $CDR_{cations}$ and CDR_{carbon} were similar, but at low values CDR_{carbon} was orders of magnitude lower than $CDR_{cations}$.

In unbuffered models, soil solution pH increased rapidly from the initial pH and then plateaued after around 2 years for all materials (Fig. 3). For the mill ashes, this corresponded with a rapid decrease in the concentration of calcium, magnesium, and potassium hydroxides/oxides followed by a gradual decrease in the concentration of potassium and plagioclase feldspars (Fig. S5). For the Tichum Creek basalt, this corresponded with a rapid decrease in the concentration of olivine followed by a gradual decrease in augite concentration (Fig. S6). Overall, soil solution pH levels increased with initial pH and decreasing pCO_2 . In constantly buffered scenarios, with soil solution pH buffered at 4.5, 5.5 or 6.5, CDR was several orders of magnitude lower than in the unbuffered scenarios (Figs. 1 and 2). However, the relative effects of pH and pCO_2 remained the same.

3.3. Reactive tranport model sensitivity analysis

The most pronounced effects on soil solution pH throughout the simulations were initial soil solution pH, pH buffering, and the interaction between these two factors and infiltration rate/transport time step duration (Fig. 4). Irrespective of plant uptake of nutrients, pCO_2 or amendment surface area, unbuffered high initial pH led to a fairly constant pH of around 7–8 throughout the simulation. In contrast, unbuffered low initial pH led to a fairly constant pH of around 5.5–6.0 under low infiltration (9.5-day time step) and a pH that fell to around 4 under high infiltration (1.8-day time step).

Cumulative CDR_{carbon} after 15 years was less sensitive to changes in most parameters than $CDR_{cations}$ (Fig. 5). The parameters with the largest absolute effect on CDR_{carbon} were pH buffering, initial soil solution pH, pCO_2 , and their interactions (Table 7). On average, high pH scenarios achieved 0.5 t CO_2/ha more CDR than low pH scenarios, and constant buffering resulted in minimal CDR_{carbon} (<0.005 t CO_2/ha ; Table 7). The parameters with the largest absolute effect on $CDR_{cations}$ were organic carbon cation exchange sites, initial pH, infiltration rate/transport time step duration, and the combined effect of initial pH and pH buffering (Table 7). All scenarios with high organic carbon cation exchange sites produced negative cumulative CDR values. In contrast, estimates of $CDR_{cations}$ were greater than the theoretical maximum (4.43 t CO_2/ha) under constantly buffered scenarios with low pH (Table S8).

Table 5

Maximum potential carbon dioxide removal (CDR) of each material based on R_{CO_2} and an application rate of 100 t wet material/ha, cumulative CDR after 15 years based on reactive transport modelling under different initial pH (unbuffered) scenarios (values italicised in brackets are given in kg/ha), and the proportion of maximum potential CDR achieved after 15 years. CDR was calculated using the sum of cations released into solution ($CDR_{cations}$) or bicarbonate generated (CDR_{carbon}). All other parameters were at moderate levels.

Material	Maximum potential CDR (t/ha)	Initial pH	Cumulative CDR after 15 years (t/ha)		Proportion of potential CDR achieved (%)	
			$CDR_{cations}$	CDR_{carbon}	$CDR_{cations}$	CDR_{carbon}
Tichum Creek basalt	31.0	4.5	17.0	13.7	54.7	44.1
		5.5	18.2	16.6	58.6	53.6
		6.5	15.8	15.8	51.0	51.1
Racecourse mill ash	5.48	4.5	1.3	0.0 (0.3)	24.0	0.0
		5.5	3.1	1.8	55.8	33.8
		6.5	3.8	3.7	70.0	67.0
Victoria mill ash	4.43	4.5	1.1	0.0 (0.9)	25.5	0.0
		5.5	2.6	1.4	58.5	32.6
		6.5	3.4	3.3	76.9	73.8
Pioneer mill ash	3.75	4.5	1.1	0.0 (0.7)	30.3	0.0
		5.5	2.7	1.6	72.3	42.0
		6.5	3.5	3.4	93.6	90.3
Tablelands mill ash	3.20	4.5	1.0	0.0 (0.7)	30.8	0.0
		5.5	2.0	1.0	62.0	29.7
		6.5	2.8	2.7	86.5	83.4
Mulgrave mill ash	2.66	4.5	0.7	0.0 (0.8)	24.6	0.0
		5.5	1.8	0.9	69.1	34.3
		6.5	2.6	2.6	99.1	97.5

Table 6

Maximum potential carbon dioxide removal (CDR) of each material based on R_{CO_2} and an application rate of 100 t wet material/ha, cumulative CDR after 15 years based on reactive transport modelling under different carbon dioxide partial pressure scenarios (values italicised in brackets are given in kg/ha), and proportion of maximum potential CDR achieved after 15 years. CDR was calculated using the sum of cations released into solution ($CDR_{cations}$) and bicarbonate generated (CDR_{carbon}). All other parameters are at moderate levels including initial soil solution pH at 5.5 and unbuffered.

Material	Maximum potential CDR (t/ha)	Carbon dioxide partial pressure	Cumulative CDR after 15 years (t/ha)		Proportion of potential CDR achieved (%)	
			$CDR_{cations}$	CDR_{carbon}	$CDR_{cations}$	CDR_{carbon}
Tichum Creek basalt	31.0	Low	4.5	2.8	14.6	9.2
		Moderate	18.2	16.6	58.6	53.6
		High	24.0	22.4	77.4	72.2
Racecourse mill ash	5.48	Low	1.8	0.1	32.6	1.8
		Moderate	3.1	1.8	55.8	33.8
		High	3.6	2.6	65.5	47.9
Victoria mill ash	4.43	Low	1.5	0.0 (9.1)	34.4	0.2
		Moderate	2.6	1.4	58.5	32.6
		High	3.1	2.2	70.2	50.7
Pioneer mill ash	3.75	Low	1.6	0.0 (34.4)	43.5	0.9
		Moderate	2.7	1.6	72.3	42.0
		High	3.2	2.4	86.4	63.1
Tablelands mill ash	3.20	Low	1.3	0.0 (2.9)	40.2	0.1
		Moderate	2.0	1.0	62.0	29.7
		High	2.5	1.7	78.0	54.1
Mulgrave mill ash	2.66	Low	1.2	0.0 (2.8)	46.7	0.1
		Moderate	1.8	0.9	69.1	34.3
		High	2.3	1.7	86.6	62.1

4. Discussion

4.1. Composition of mill ashes

Overall, the mill ashes were broadly similar in composition, but there were differences. The differences could be due to variability in boiler conditions during combustion of bagasse, as well as regional differences in the extraneous matter (soil and leaves). Reported boiler temperatures generally range from 400 to 800 °C. The presence of melted amorphous silicate material and the inverse relationship between crystalline and amorphous silicon (Fig. S1; Table 3) indicates substantial melting of quartz and other minerals at temperatures above 900 °C, similar to previous studies (Clark et al., 2017; Soltani et al., 2015). However, the presence of inorganic carbon in four out of five mill ashes (Table 2) suggested that parts of the boilers did not sustain temperatures in or above the range in which carbonates undergo thermal decomposition (500–900 °C). Alternatively, it is possible that carbonate was generated

by weathering in the stockpile, given that temperature and water content were high. However, it does appear that conditions vary within boilers. Regional differences in the amount of extraneous matter collected with the cane and processed into bagasse will also affect mill ash composition. Soil contains crystalline silicates such as quartz, illite/muscovite and potassium feldspar whereas cane leaves contain amorphous silica phytoliths (Negão and Driemeier, 2022). The amount and type of extraneous matter depends on the speed and setting of the harvester (farm-scale differences), the type and wetness of the soil at harvest (regional differences in weather and climate), and whether the cane is burned prior to harvest or harvested green (regional differences in management; Larsen et al., 2017; Patane et al., 2019).

4.2. Carbon dioxide removal potential of mill ashes

The five mill ashes analysed in this study tended to have higher concentrations of calcium, magnesium, potassium, and sodium than

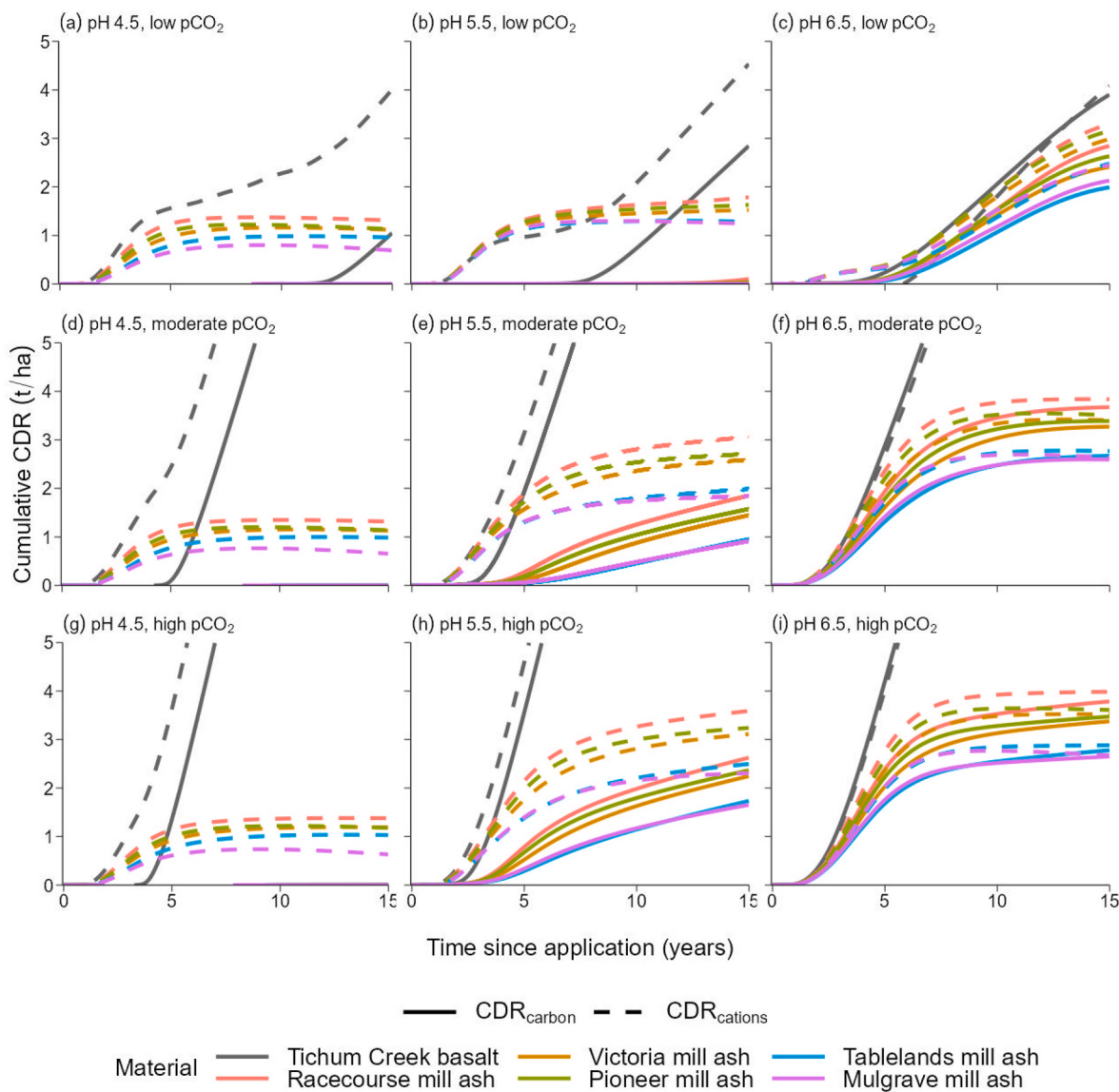


Fig. 1. Cumulative tonnes of carbon dioxide removed, calculated using the sum of bicarbonate produced ($\text{CDR}_{\text{carbon}}$) and the sum of cations released into solution ($\text{CDR}_{\text{cations}}$), per hectare over 15 years for each material in the unbuffered simulations. Columns represent scenarios where initial soil solution pH is a) 4.5, b) 5.5, and c) 6.5. Rows represent scenarios where the carbon dioxide partial pressure ($p\text{CO}_2$) of the soil profile is a) low, d) moderate, and g) high. All other parameters are at moderate levels. Cumulative CDR values after 15 years for Tichum Creek basalt (cut off in some plots) are in Table S7. In plots where full lines ($\text{CDR}_{\text{carbon}}$) are not visible it is because the values are close to zero.

previously reported for other mill ashes, with sodium not previously measured or detected (Table S1). As a result, the theoretical maximum CDR potential of the five ashes used in this study was greater than expected. There were no clear geographical effects on composition, so differences were more likely due to variations in mill boiler characteristics and operation, and techniques of storage, sampling, and analysis.

4.3. Carbon dioxide removal of mill ashes compared to basalt and analogues in nature

Under the various scenarios modelled, weathering of wet mill ash resulted in significantly lower CDR than weathering of Tichum Creek basalt. Furthermore, cumulative CDR from weathering of the basalt did not plateau in the 15-year period simulated (Figs. 1 and 2), indicating further CDR potential over time. Despite this, mill ash may still be a highly effective material for CDR via EW. Weathering of the Racecourse mill ash removed 4.0 t CO_2/ha under the unbuffered, high initial soil solution pH, high $p\text{CO}_2$ scenario, with different ashes producing similar

results (Figs. 1 and 2). This is equivalent to 0.040 t CO_2/t wet ash which is comparable to the Cragmill and Tawau basalts modelled by Lewis et al. (2021), which removed 0.026 and 0.060 t CO_2/t material, respectively, and to modelled estimates for other basalts and olivine (Rinder and von Hagke, 2021; Vienne et al., 2022; Pogge von Strandmann et al., 2022; Cipolla et al., 2021). Additionally, this level of CDR was achieved in a relatively short timeframe (around 5 years) where previous studies of olivine have predicted that the CDR benefits may take decades to centuries to eventuate (Cipolla et al., 2021; Hartmann et al., 2013). The relatively rapid CDR in mill ashes most likely reflects the high proportion of fast weathering oxide and hydroxide minerals in them compared to slower weathering minerals like potassium feldspar and augite in the basalt (Figs. S5–S6). It may also be the result of the high SSA of the mill ashes compared to the basalt, although our sensitivity analysis (Table 7) and the modelling of Lewis et al. (2021) indicate that mineralogy and soil solution pH are more influential.

It is expected that lifecycle benefits (e.g., recycling of industrial by-products, shorter transport distances) may make mill ash equivalent

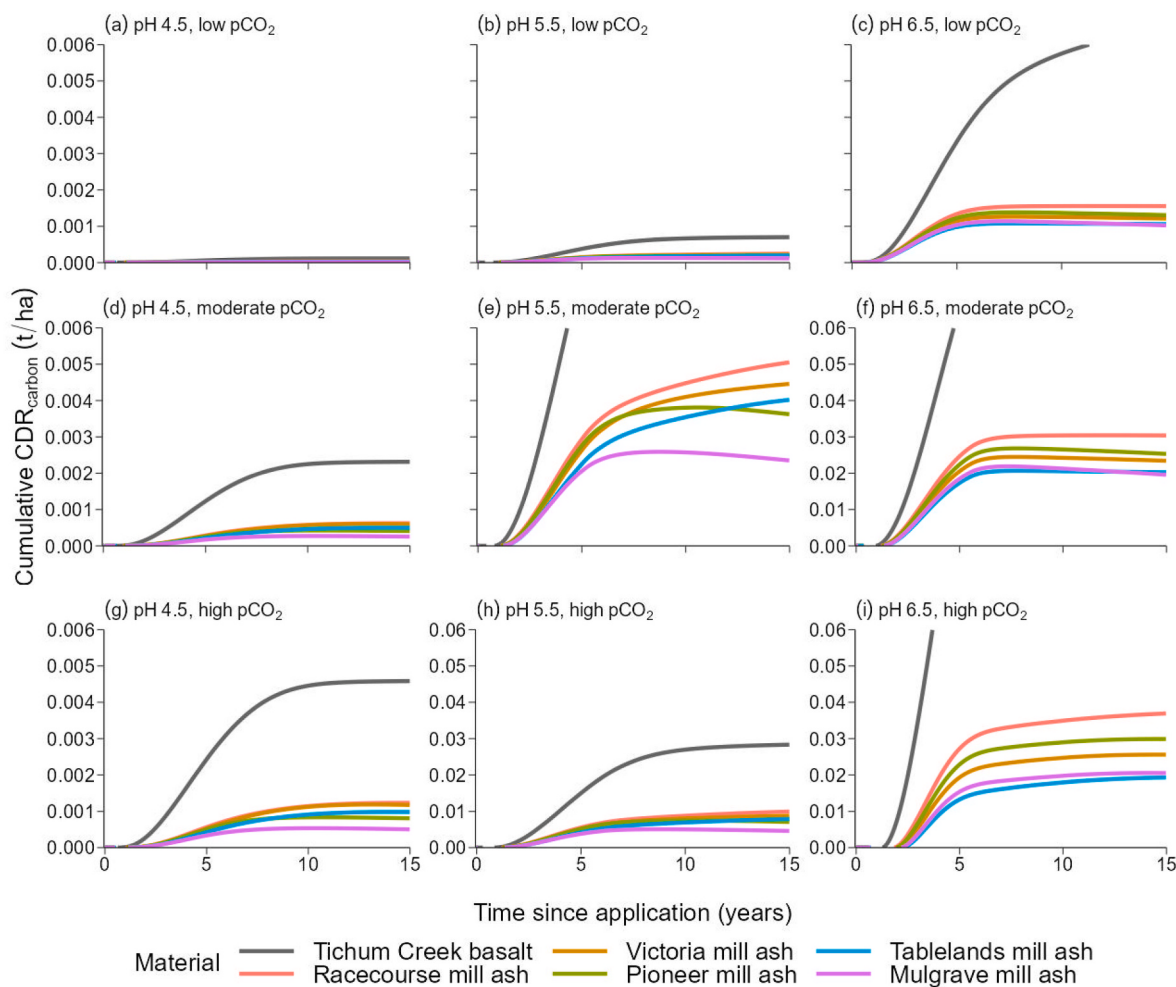


Fig. 2. Cumulative tonnes of carbon dioxide removed, calculated using the sum of bicarbonate produced ($\text{CDR}_{\text{carbon}}$), per hectare over 15 years for each material in constantly buffered simulations. Columns represent scenarios in which soil solution pH is buffered at a) 4.5, b) 5.5, and c) 6.5. Rows represent scenarios where the carbon dioxide partial pressure (pCO_2) of the soil profile is a) low, d) moderate, and g) high. All other parameters are at moderate levels. Note the change in y axis scale compared to Fig. 1, and in panels f, h, and i.

and potentially preferable to mined rock alternatives. Given the high proportion of water in mill ash (around 50%; Table 3), dewatering could increase transport efficiency and therefore CDR over the lifecycle of the mill ash although the energy required may be too high. Additionally, if assessed as a dry material, the cumulative CDR of the mill ashes can be expected to almost double. Mill ash could be reapplied when cumulative CDR plateaus, and that time period more-or-less corresponds with the length of a crop cycle, so applications could be incorporated with the cultivation that occurs between crop cycles. However, the effect of repeated applications on soil chemistry over time needs to be assessed.

While modelled CDR from weathering of mill ash compares favourably to that of basalt, it is worth comparing the modelled values to the likely maximum value possible. This can be estimated from measurements of dissolved inorganic carbon exported in rivers draining catchments comprised of easily weathered recently deposited volcanic ash, with a hot wet climate. The highest such value reported is 2.82 t CO₂/ha/year in Java (Dessert et al., 2003). Actual CDR via EW of comparably small amounts of weatherable material applied to land is unlikely to exceed this value and as stated previously, our models represent extremes that bracket likely CDR in the field.

4.4. Effect of soil solution pH and carbon dioxide partial pressure on carbon dioxide removal

The sum of cations released into solution has frequently been used to

estimate CDR, but our results show the degree to which that overestimates CDR under realistic conditions of soil pH and pCO_2 . Mineral weathering by carbonic acid (the main acid present in moderately acidic soils) consumes carbon dioxide, whereas weathering by stronger acids such as sulfuric, nitric, and some organic acids (in acidic soils) does not (Hartmann et al., 2013; Taylor et al., 2021; Bertagni and Porporato, 2022; Dietzen and Rosing, 2023). This is evident in our study as $\text{CDR}_{\text{carbon}}$ was consistently lower than $\text{CDR}_{\text{cations}}$ (Tables 5 and 6). Furthermore, predicted CDR was orders of magnitude less when pH was kept low in constantly buffered scenarios (Fig. 1) as may occur during nitrification following nitrogen fertiliser application (Fig. 6; Hartmann et al., 2013; Taylor et al., 2021). Dietzen and Rosing (2023) concluded that CDR estimates based on cations released require correction for weathering by non-carbonic acids where soil solution pH is less than 6.3, assuming constant pH over time. We calculated their correction factor (X^*) for scenarios modelled here by substituting our three pH levels while keeping pCO_2 at the average level across the profile in the moderate scenario (see Dietzen and Rosing, 2023, Supplementary Material spreadsheet). According to this correction factor, $\text{CDR}_{\text{carbon}}$ should increase from 9–91 to 100% of $\text{CDR}_{\text{cations}}$ as pH increases from 4.5 to 5.5 to 6.5. Our modelling found even greater differences between $\text{CDR}_{\text{cations}}$ and $\text{CDR}_{\text{carbon}}$ especially at pH 4.5 and 5.5 (Table 5) and in our constantly buffered models (Table S8) which include more geochemical reactions than the models of Dietzen and Rosing (2023). This indicates an even greater correction for strong acid weathering and further

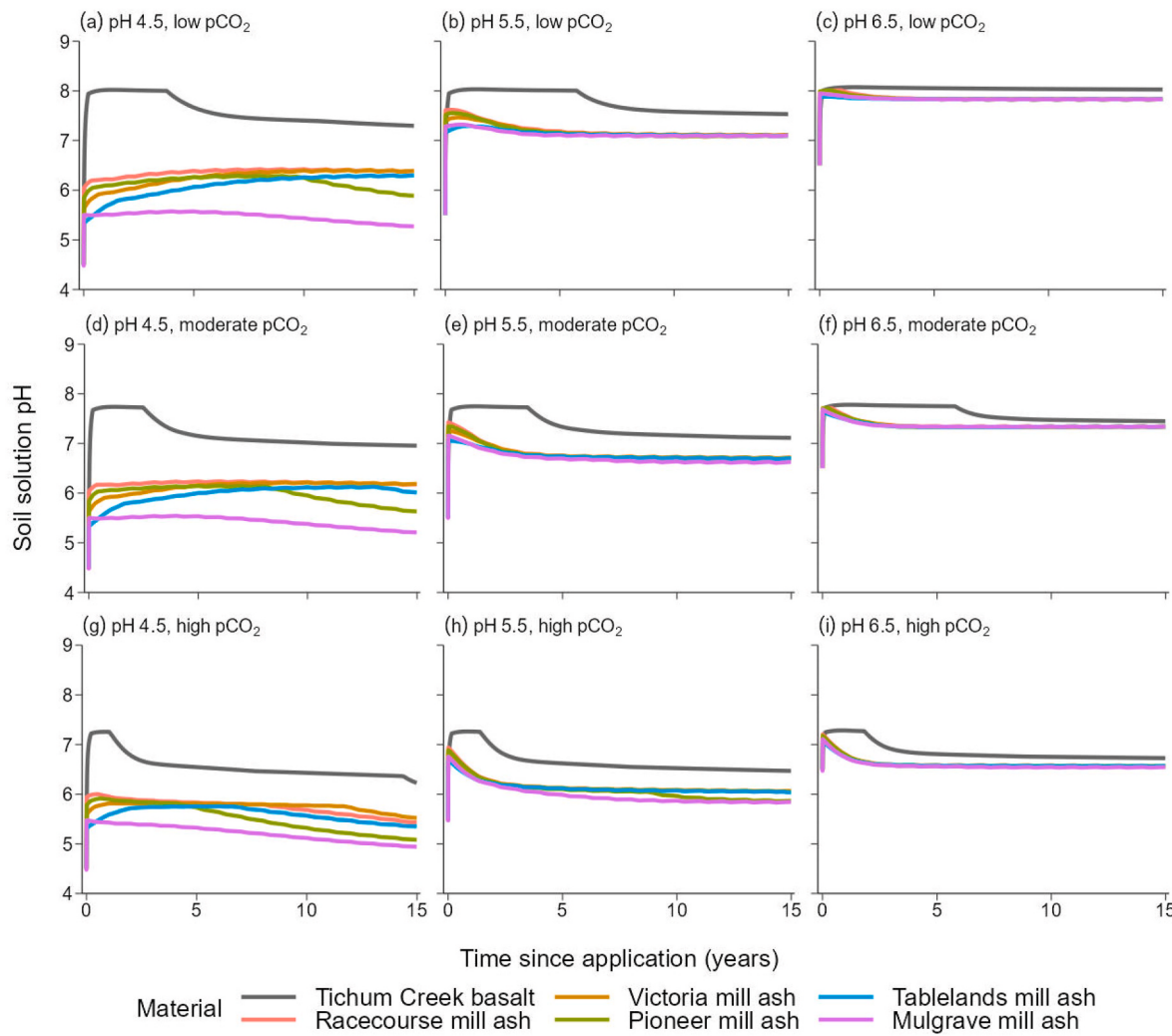


Fig. 3. Soil solution pH over 15 years for each material in the unbuffered simulations. Columns represent scenarios where initial soil solution pH is a) 4.5, b) 5.5, and c) 6.5. Rows represent scenarios where the carbon dioxide partial pressure ($p\text{CO}_2$) of the soil profile is a) low, d) moderate, and g) high. All other parameters are at moderate levels.

interrogation of the reactive transport model may be warranted (see Section 4.5 Reactive transport model sensitivity analysis and general limitations).

Changes in soil solution pH resulting from weathering in the field will be initially buffered by changes in variable charge, cation exchange reactions and other processes such as conversion between exchangeable Al^{3+} and aluminium hydroxides (Fig. 6). However, pH is expected to increase gradually over time, providing alkalinity is generated more rapidly than acidity. Therefore, the evolution of soil pH following application of amendments could be expected to track somewhere between our unbuffered and constantly buffered models (for a given initial pH). We calculated the expected change in pH given the maximum amount of bicarbonate generated in unbuffered models i.e., calculated using the sum of cations released, using pH buffering capacities of real soils (Wang et al., 2014). For the Tablelands mill ash, the expected pH change ranged from 0.29 to 2.14 units over 15 years (Tables S9–S10) with most of the change occurring between 3 and 5 years after application. This corresponds with a field trial that found ash applications of 150 t/ha raised soil pH from 6.25 (in the control) to 6.43 after the second ratoon (Kingston, 1999). In summary, soil pH has important implications for CDR predictions, and future reactive transport models should attempt more realistic simulation of acid/alkali inputs/outputs and soil pH buffering mechanisms.

There are very few published results of CDR via EW in field trials. In a

small-catchment-scale field trial in Malaysia, with annual applications of zero or 50 t/ha of basalt, Larkin et al. (2022) measured CDR of 0.00–0.51 t CO_2/ha as pedogenic carbonates over 3 years, but none of that was attributable to the basalt treatment, and there was no measurable effect of basalt application on bicarbonate export in stream water. In a catchment study in the USA, Taylor et al. (2021) measured CDR of 0.025–0.13 t CO_2/ha as stream water bicarbonate over 15 years following a single application of 3.4 t/ha of wollastonite. These results are equivalent to 0.0000–0.0034 and 0.0073–0.0378 t CO_2/t material, respectively, encompassing the range of $\text{CDR}_{\text{carbon}}$ values modelled for mill ash in our study (0.0000–0.0398 t CO_2/t wet ash). Note that values measured in the field are orders of magnitude less than several published modelled estimates based on the sum of cations released. The presence of strong acid is likely to have limited CDR in these field studies as soil pH was reported as less than 5.1 in both. Higher soil pH, longer trial duration and more weatherable and cation-rich material presumably accounted for higher CDR per tonne of material found by Taylor et al. (2021). In our modelling, CDR from weathering of the Tichum Creek basalt took between 5 and 12 years to begin for soils with pH of 4.5 (Fig. 1). Additionally, reactions between weathering products and ground- and stream water likely reduced CDR in these field studies (Renforth and Henderson, 2017) and we did not model transport beyond the bottom of the soil profile. Critically, too few studies exist currently to understand factors affecting CDR via EW in the field, particularly across

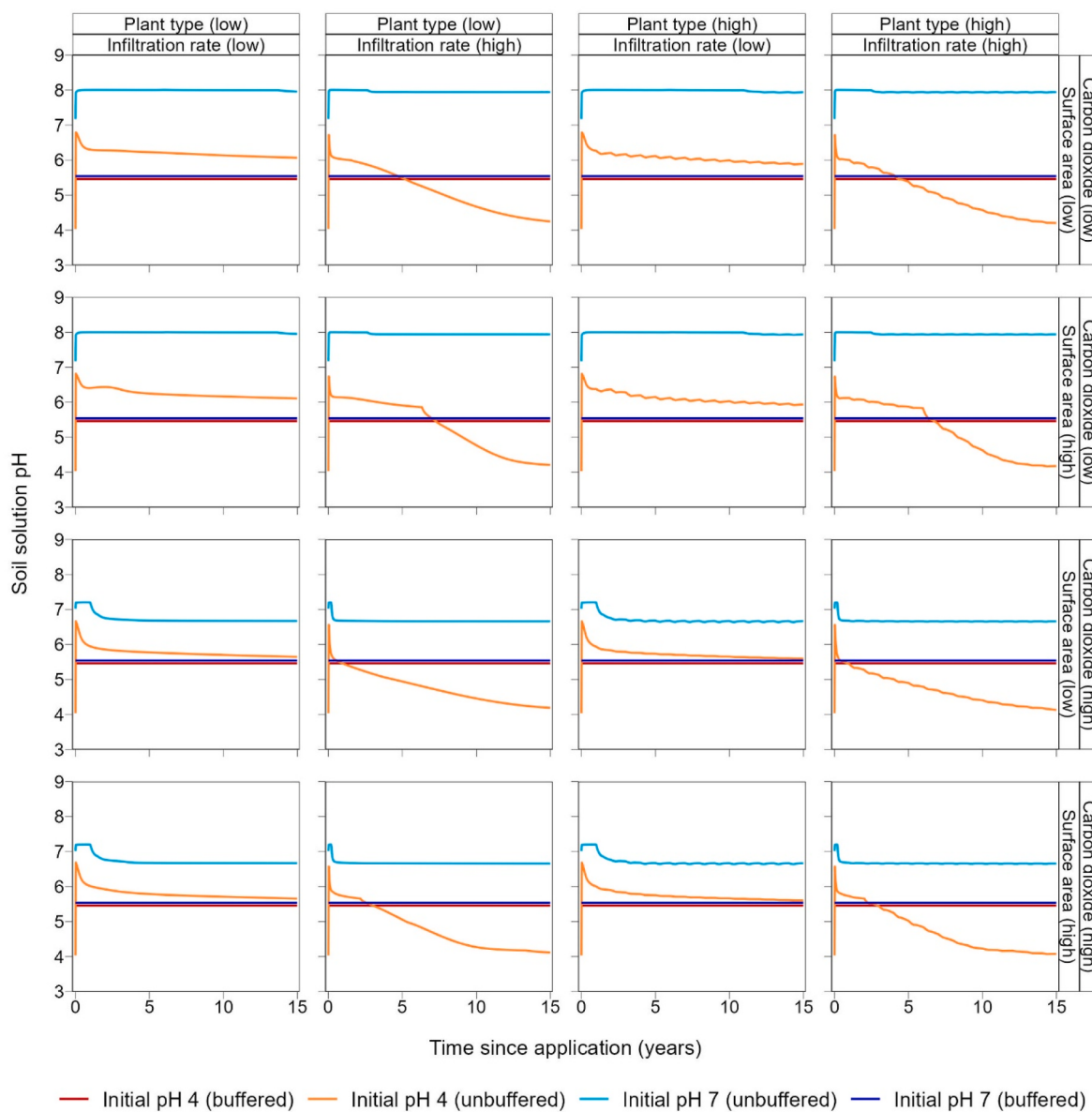


Fig. 4. Soil solution pH over 15 years in sensitivity analysis scenarios. Factor levels are defined in Table S6. The high and low initial soil solution pH lines overlap in constantly buffered (5.5) scenarios, and are included for completeness.

soil types and agricultural systems and over extended time periods.

Based on this geochemical modelling, EW for CDR is most likely to be effective in soils with relatively high pH (~6.5) or soils with lower pH (~5.5–6.5) but having high pCO₂; new field trials should focus on those situations. Up to 3.6 t CO₂/ha was removed via weathering of mill ash under the high pCO₂ scenario when initial soil solution pH was at 5.5 and unbuffered (Table 6). This may reflect conditions in some tropical soils where pH is low, but organic matter inputs, moisture content and temperature are high, facilitating biological activity and elevated carbon dioxide concentrations. Application of decomposable organic materials together with weatherable inorganic materials is relevant to sugarcane growing areas, as mill ash is often mixed with mill mud or press mud, another sugarcane mill by-product that has high organic matter content (~30% of dry weight; Moody et al., 2014; Prado et al., 2013). However, the possible beneficial effect of mill mud on CDR by weathering needs validation in the field as the release of carbon dioxide through organic matter decomposition may be too rapid for timescales relevant to weathering (Denmead et al., 2008; Nguyen et al., 2014). Additionally, minimal CDR was modelled when pH was 4.5, even at the highest pCO₂

(Table 6). This reflects the predictions of Bertagni and Porporato (2022) and Dietzen and Rosing (2023) that below pH 5.2, the presence of strong acids will outweigh the effect of increasing pCO₂ and significantly limit CDR. In contrast, above pH 7.1, carbonate precipitation can release substantial amounts of carbon dioxide. This was the case for Tichum Creek basalt in this study (up to 3.5 t CO₂/ha) but not for mill ashes even under high pH conditions (Table S5; Fig. S2).

4.5. Reactive transport model sensitivity analysis and general limitations

Changing model parameters generally had less of an effect on CDR_{carbon} than CDR_{cations}. This is likely because CDR_{carbon} was generally lower (Tables 5 and 6). Estimates of CDR, particularly CDR_{carbon}, were most affected by pH buffering, initial pH, pCO₂, and their interactions. This was evident from the main analysis presented in our study and has been discussed already. In contrast, CDR_{cations} was most affected by organic carbon cation exchange sites and initial soil solution pH, although higher CDR_{cations} was expected at lower pH due to increased weathering rates. In our modelling, we did see the expected relationship

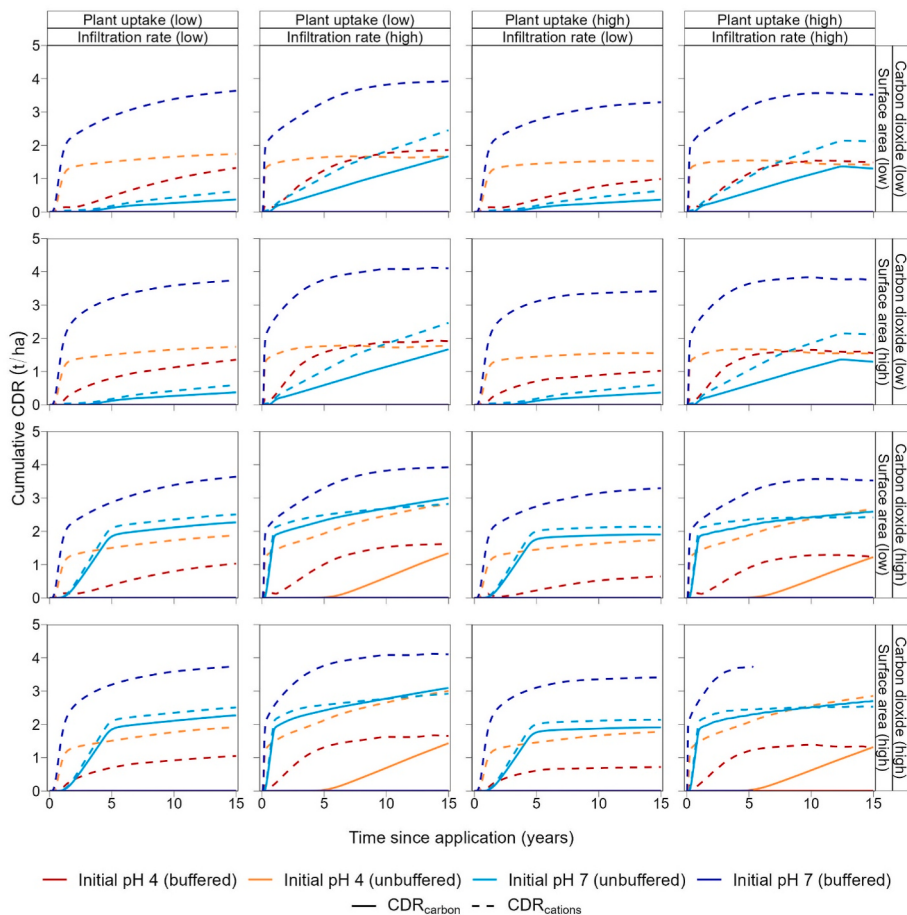


Fig. 5. Cumulative tonnes of carbon dioxide removed ($\text{CDR}_{\text{carbon}}$ and $\text{CDR}_{\text{cations}}$) per hectare over 15 years in sensitivity analysis scenarios. Factor levels are defined in Table S6. Values for $\text{CDR}_{\text{carbon}}$ and $\text{CDR}_{\text{cations}}$ under high organic carbon cation exchange site scenarios were negative and are not shown. Values for $\text{CDR}_{\text{carbon}}$ under pH buffering scenarios were also negative.

Table 7

Results of sensitivity analysis of main factor effects for parameters tested and key interactions on carbon dioxide removal (CDR). Negative effect size values indicate the high factor level achieved less CDR on average than the low factor level. The high factor level for initial soil solution pH is 7 and the low level is 4. All factor levels are defined in Table S6.

Factor	Effect size (t CO ₂ /ha)	
	CDR _{cations}	CDR _{carbon}
Initial soil solution pH	1.29	0.52
Presence/absence of pH buffering	0.43	-0.69
Mill ash surface area	0.07	0.01
Carbon dioxide partial pressure	0.26	0.40
Organic carbon cation exchange sites	-1.60	-0.33
Plant uptake of nutrients	-0.17	-0.05
Infiltration rate/transport time step duration	0.91	0.38
Initial soil solution pH x Presence/absence of pH buffering	0.92	-0.52
Initial soil solution pH x Carbon dioxide partial pressure	0.15	0.23
Presence/absence of pH buffering x Carbon dioxide partial pressure	-0.35	-0.40
Initial soil solution pH x Presence/absence of pH buffering x Carbon dioxide partial pressure	0.18	-0.54

between pH and weathering rate in both buffered and unbuffered scenarios (Figs. S5–S6). This is particularly evident for potassium feldspar in the mill ashes and augite in the basalt. However, the expected relationship between pH and $\text{CDR}_{\text{cations}}$ was not seen. Instead, the highest $\text{CDR}_{\text{cations}}$ was achieved at low pH with impossibly high predictions $\text{CDR}_{\text{cations}}$ under constantly buffered low pH scenarios (Tables 5 and S8,

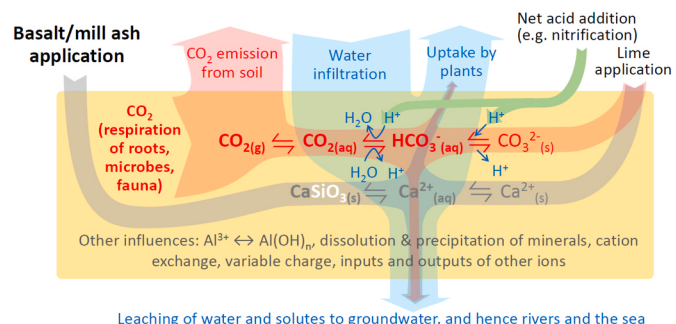


Fig. 6. Factors influencing the capture of carbon dioxide via enhanced weathering in agricultural soil (yellow rectangle). Blue indicates water fluxes, red indicates carbon fluxes and the carbonate equilibrium, and grey indicates alkali or alkaline-earth metal (e.g., calcium) phases and fluxes.

Fig. 1). These results can be explained by exploring exchange surface chemistry. In the model, exchange surfaces are initially filled with Ca^{2+} , Mg^{2+} , Na^+ , and H^+ ions in equilibrium with the background solution. In unbuffered models, Ca^{2+} and Mg^{2+} released via weathering displace exchangeable H^+ , which is then leached from the profile, increasing soil solution pH. In constantly buffered models, H^+ ions are added to counteract the increase in pH, shifting the baseline equilibrium further, leaving fewer exchanges sites to which Ca^{2+} and Mg^{2+} (in the background solution and released via weathering) can adsorb. As such, the greater the increase in pH, the more calcium and magnesium is

transported out of the profile. Weathering models with low initial pH had large increases in pH (2–3 units) whereas blank models had relatively stable pH (Fig. S7). This inflated the difference in cations transported to the bottom of low pH weathering and blank profiles, with or without constant buffering, resulted in unrealistic CDR_{cations} values (Fig. S8), and led to slight decreases in cumulative CDR_{carbon} in the last 5–10 years of some scenarios (Fig. 2). This likely also explains negative CDR values predicted under scenarios with high concentrations of organic carbon cation exchange sites and reinforces the need for better modelling of soil solution pH buffering mechanisms and cation exchange surfaces. It also highlights a general limitation of calculating carbon removal by difference between a control soil which differs in multiple complex ways from amended soils.

Infiltration rate also had a notable effect on CDR, particularly CDR_{cations}. In reality, this parameter represents the difference between infiltration of water into the soil profile and uptake/evapotranspiration so should be considered water flux rather than the infiltration rate. Below the root zone i.e., at the bottom of the profile where we calculate CDR, this movement of water represents deep drainage. Higher water flux results in shorter time steps and faster transport of weathering products out of the profile. This prevents reaction saturation and secondary reactions (e.g., with exchange surfaces), resulting in more weathering. However, the rapid increase in CDR to above 1.5 t CO₂/ha in around 2 years may be unrealistic (Fig. 5). In contrast, our low infiltration rate scenarios reiterate the limited potential for CDR in arid and semi-arid climates in the absence of irrigation (<900 mm/year; Calabrese et al., 2022; Cipolla et al., 2021). Simulated CDR would have been even lower if water content had not been held constant but had been allowed to drop in response to lower infiltration. Our results highlight the importance of site-specific hydrodynamics in geochemical models. Furthermore, crop type has been found to significantly affect CDR (Cipolla et al., 2022; Taylor et al., 2017) although the effect of plant nutrient uptake in our study was minimal. Similarly, the effect of temperature been found to be important but was not explored here (Baek et al., 2023; Haque et al., 2023). The impacts of plant growth and land management practices on carbon and nitrogen cycles were not modelled.

5. Conclusions

Our study was the first to assess the potential for CDR via EW of sugarcane mill ash using established geochemical models. Soil pH and pCO₂ had a significant effect on CDR, resulting in estimates of 0.0–4.0 t CO₂/ha following application of 100 t/ha of wet mill ash. The maximum CDR was comparable to previously modelled mined rock alternatives and was achieved in a relatively short amount of time (around 5 years). This suggests mill ash is a promising material for CDR via EW, especially if lifecycle benefits are taken into account.

Estimates of CDR were substantially affected by the method of calculation and by several variables, with several implications for modelling. Tracing carbon from carbon dioxide to bicarbonate revealed lower sequestration rates than previous models have suggested and cast doubt on the assumption that CDR via EW will be high in acidic tropical soils. Our estimates of CDR correspond with the results of the few field studies that have been published to date. Furthermore, our sensitivity analysis highlighted limitations of the geochemical model used, particularly regarding pH buffering and cation exchange mechanisms. To provide sufficient accuracy for predicting the effectiveness of CDR via EW, and for monitoring, reporting, and verification (MRV) of commercial projects, geochemical models of CDR via EW should take into account soil pH, pH buffering, infiltration rate, and pCO₂.

More field trials measuring actual CDR via weathering of mill ash (and silicate rocks) are necessary, and it appears the highest potential would be at sites with moderately acidic soil pH and high rainfall or irrigation. The effects of repeated applications and raising pCO₂ through removing limitations to plant growth, or addition of organic matter such

as mill mud, should also be explored.

Funding sources

This work was supported by Sugar Research Australia [grant number 2021/101] and James Cook University.

CRediT authorship contribution statement

Hannah Green: Conceptualization, Data curation, Formal analysis, Investigation, Methodology, Visualization, Writing – original draft, Writing – review & editing. **Peter Larsen:** Conceptualization, Methodology, Supervision, Writing – review & editing. **Yang Liu:** Conceptualization, Methodology, Supervision, Writing – review & editing. **Paul N. Nelson:** Conceptualization, Methodology, Supervision, Writing – review & editing.

Declaration of competing interest

The authors declare the following financial interests/personal relationships which may be considered as potential competing interests:

Hannah Green reports financial support was provided by Sugar Research Australia Ltd. Peter Larsen reports a relationship with Wilmar International Ltd that includes: employment.

Data availability

I have attached my code in the Attach Files step

Acknowledgements

We are grateful to Peter Wade, Amy Lewis and Lyla Taylor for their advice and assistance with the reactive transport model, Lyla Taylor for providing feedback on the manuscript, the Advanced Analytical Centre at James Cook University for undertaking chemical analyses, Scott Smithers for his assistance with particle size analysis, Wilmar Sugar, Mackay Sugar Limited, and MSF Sugar for supplying sugarcane mill ash, the Australian Government for their support through an Australian Government Research Training Program Scholarship, and Sugar Research Australia for their support through a Postgraduate Research Scholarship.

Appendix A. Supplementary data

Supplementary data to this article can be found online at <https://doi.org/10.1016/j.apgeochem.2024.105940>.

References

- Akaike, H., 1973. Information theory and an extension of the maximum likelihood principle. In: Springer Series in Statistics. Springer New York, New York, NY, pp. 610–624.
- Amann, T., Hartmann, J., 2019. Ideas and perspectives: synergies from co-deployment of negative emission technologies. Biogeosciences 16 (15), 2949–2960.
- Amann, T., Hartmann, J., Struyf, E., de Oliveira Garcia, W., Fischer, E.K., Janssens, I., Meire, P., Schoelynck, J., 2020. Enhanced weathering and related element fluxes – a cropland mesocosm approach. Biogeosciences 17 (1), 103–119.
- Amundson, R.G., Davidson, E.A., 1990. Carbon dioxide and nitrogenous gases in the soil atmosphere. J. Geochim. Explor. 38 (1–2), 13–41.
- Andrews, M.G., Taylor, L.L., 2019. Combating climate change through enhanced weathering of agricultural soils. Elements 15 (4), 253–258. <https://doi.org/10.2138/gselements.15.4.253>.
- Appelo, C.A.J., Postma, D., 2005. Geochemistry, Groundwater and Pollution, 2nd ed. CRC Press, Taylor & Francis Group, London, UK.
- Aradóttir, E.S.P., Sonnenthal, E.L., Jónsson, H., 2012. Development and evaluation of a thermodynamic dataset for phases of interest in CO₂ mineral sequestration in basaltic rocks. Chem. Geol. 304–305, 26–38.
- Ascough, P.L., Bird, M.I., Brock, F., Higham, T.F.G., Meredith, W., Snape, C.E., Vane, C. H., 2009. Hydrolysis as a new tool for radiocarbon pre-treatment and the quantification of black carbon. Quat. Geochronol. 4 (2), 140–147. <https://doi.org/10.1016/j.quageo.2008.11.001>.

- Baek, S.H., Kanzaki, Y., Lora, J.M., Planavsky, N., Reinhard, C.T., Zhang, S., 2023. Impact of climate on the global capacity for enhanced rock weathering on croplands. *Earth's Future* 11, e2023EF003698. <https://doi.org/10.1029/2023EF003698>.
- Barry, G.A., Price, A.M., Lynch, P.J., 1998. Some implications of the recycling of sugar industry by-products. *Proc. Aust. Soc. Sugar Cane Technol.* 20, 52–55.
- Barry, G.A., Rayment, G.E., Jeffrey, A.J., Price, A.M., 2001. Changes in cane soil properties from applications of sugarmill by-products. *Proc. Aust. Soc. Sugar Cane Technol.* 23, 185–191.
- Beerling, D.J., Leake, J.R., Long, S.P., Scholes, J.D., Ton, J., Nelson, P.N., Bird, M.I., Kantzas, E., Taylor, L.L., Sarkar, B., Kelland, M., DeLucia, E., Kantola, I.B., Müller, C., Rau, G., Hansen, J., 2018. Farming with crops and rocks to address global climate, food and soil security. *Nat. Plants* 4 (3), 138–147.
- Benshara, M., Telford, R., Stern, B., Gaffney, V., 2022. Loss on ignition vs. thermogravimetric analysis: A comparative study to determine organic matter and carbonate content in sediments. *J. Paleolimnol.* 67 (2), 191–197.
- Bertagni, M.B., Porporato, A., 2022. The carbon-capture efficiency of natural water alkalization: implications for enhanced weathering. *Sci. Total Environ.* 838 (4), 156524.
- Berthelsen, S., Hurney, A., Kingston, G., Rudd, A., Garside, A.L., Noble, A.D., 2001. Plant cane responses to silicated products in the Mossman, Innisfail and Bunderberg districts. *Proc. Aust. Soc. Sugar Cane Technol.* 23, 297–303.
- Blanc, P., Lassin, A., Piantone, P., Azaroual, M., Jacquemet, N., Fabbri, A., Gaucher, E.C., 2012. Thermodem: a geochemical database focused on low temperature water/rock interactions and waste materials. *Appl. Geochem.* 27 (10), 2107–2116.
- Blecker, S.W., McCulley, R.L., Chadwick, O.A., Kelly, E.F., 2006. Biologic cycling of silica across a grassland bioclimosequence. *Global Biogeochem. Cycles* 20 (3).
- Bobicki, E.R., Liu, Q., Xu, Z., Zeng, H., 2012. Carbon capture and storage using alkaline industrial wastes. *Prog. Energy Combust. Sci.* 38 (2), 302–320.
- Brooks, M.E., Kristensen, K., van Bentem, K.J., Magnusson, A., Berg, C.W., Nielsen, A., Skauge, H.J., Maechler, M., Bolker, B.M., 2017. glmmTMB balances speed and flexibility among packages for zero-inflated generalized linear mixed modeling. *The R Journal* 9 (2), 378–400. <https://cran.r-project.org/package=glmmTMB>.
- Bruce, R.C., Warrell, L.A., Bell, L.C., Edwards, D.G., 1989. Chemical attributes of some Queensland acid soils I, Solid and solution phase compositions. *Aust. J. Soil Res.* 27 (2), 333–351.
- Brunauer, S., Emmett, P.H., Teller, E., 1938. Adsorption of gases in multimolecular layers. *J. Am. Chem. Soc.* 60 (2), 309–319.
- Buckingham, F.L., Henderson, G.M., Holdship, P., Renforth, P., 2022. Soil core study indicates limited CO₂ removal by enhanced weathering in dry croplands in the UK. *Appl. Geochem.* 147, 105482.
- Calabrese, S., Wild, B., Bertagni, M.B., Bourg, I.C., White, C., Aburto, F., Cipolla, G., Noto, L.V., Porporato, A., 2022. Nano to global-scale uncertainties in terrestrial enhanced weathering. *Environ. Sci. Technol.* 56, 5261–15272.
- Cipolla, G., Calabrese, S., Noto, L.V., Porporato, A., 2021. The role of hydrology on enhanced weathering for carbon sequestration II. From hydroclimatic scenarios to carbon-sequestration efficiencies. *Adv. Water Resour.* 154, 103949.
- Cipolla, G., Calabrese, S., Porporato, A., Noto, L., 2022. Effects of precipitation seasonality, vegetation cycle, and irrigation on enhanced weathering. *Biogeosciences* 4, 3877–3896. <https://doi.org/10.5194/bg-19-3877-2022>.
- Clark, M.W., Despland, L.M., Lake, N.J., Yee, L.H., Anstoetz, M., Arif, E., Parr, J.F., Doumit, P., 2017. High-efficiency cogeneration boiler bagasse-ash geochemistry and mineralogical change effects on the potential reuse in synthetic zeolites, geopolymers, cements, mortars, and concretes. *Heliyon* 3 (4), e00294.
- Connor, S., 2012. Movement of Nitrogen through a Riparian Forest in a Tropical Agricultural Landscape. James Cook University.
- Dietzen, C., Rosing, M.T., 2023. Quantification of CO₂ uptake by enhanced weathering of silicate minerals applied to acidic soils. *Int. J. Greenh. Gas Control* 125 (2023), 103872.
- Denmead, O.T., Macdonald, B.C.T., Naylor, T., Wang, W., Salter, B., White, I., Wilson, S.A., Griffith, D.W.T., Moody, P., 2008. Whole-of-season greenhouse gas emissions from Australian sugarcane soils. *Proc. Aust. Soc. Sugar Cane Technol.* 30, 105–114.
- Dessert, C., Dupré, B., Gaillardet, J., Francois, L.M., Allegre, C.J., 2003. Basalt weathering laws and the impact of basalt weathering on the global carbon cycle. *Chem. Geol.* 202, 257–273.
- d'Hotman, D., de Villiers, O., 1961. Soil rejuvenation with crushed basalt in Mauritius. Part I: consistent results of worldwide interest. *Int. Sugar J.* 63, 363–364.
- Dupla, X., Möller, B., Baveye, P.C., Grand, S., 2023. Potential accumulation of toxic trace elements in soils during enhanced rock weathering. *Eur. J. Soil Sci.* 74 (1) <https://doi.org/10.1111/ejss.13343>.
- Edwards, D.P., Lim, F., James, R.I.H., Pearce, C.R., Scholes, J., Freckleton, R.P., Beerling, D.J., 2017. Climate change mitigation: potential benefits and pitfalls of enhanced rock weathering in tropical agriculture. *Biol. Lett.* 13 (4).
- Flaathen, T.K., Gislason, S.R., Oelkers, E.H., 2010. The effect of aqueous sulphate on basaltic glass dissolution rates. *Chem. Geol.* 277 (3–4), 345–354.
- Friás, M., Villar, E., Savastano, H., 2011. Brazilian sugar cane bagasse ashes from the cogeneration industry as active pozzolans for cement manufacture. *Cement Concr. Compos.* 33 (4), 490–496. <https://doi.org/10.1016/j.cemconcomp.2011.02.003>.
- Fuss, S., Lamb, W.F., Callaghan, M.W., Hilaire, J., Creutzig, F., Amann, T., Beringer, T., de Oliveira Garcia, W., Hartmann, J., Khanna, T., Luderer, G., Nemet, G.F., Rogelj, J., Smith, P., Vicente, J.L.V., Wilcox, J., del Mar Zamora Dominguez, M., Minx, J.C., 2018. Negative emissions-Part 2: costs, potentials and side effects. *Environ. Res. Lett.* 13 (6), 63002.
- Gasser, T., Guivarc, C., Tachiiri, K., Jones, C.D., Caias, P., 2015. Negative emissions physically needed to keep global warming below 2 °C. *Nat. Commun.* 6 (1), 7958.
- Haque, F., Khalid, R., Chiang, Y.W., Santos, R.M., 2023. Constraining the capacity of global croplands to CO₂ drawdown via mineral weathering. *ACS Earth Space Chem.* 7 (7), 1294–1305.
- Hartmann, J., West, A.J., Renforth, P., Köhler, P., De La Rocha, C.L., Wolf-Gladrow, D.A., Dürr, H.H., Scheffran, J., 2013. Enhanced chemical weathering as a geoengineering strategy to reduce atmospheric carbon dioxide, supply nutrients, and mitigate ocean acidification. *Rev. Geophys.* 51 (2), 113–149.
- Hartig, F., 2022. In: DHARMA: Residual Diagnostics for Hierarchical (Multi-level/mixed) Regression Models. R package version 0.4.5.
- Hepburn, C., Adlen, E., Beddington, J., Carter, E.A., Fuss, S., Mac Dowell, N., Minx, J.C., Smith, P., Williams, C.K., 2019. The technological and economic prospects for CO₂ utilization and removal. *Nature* 575 (7781), 87–97.
- Jordan, C.A., Akay, G., 2012. Speciation and distribution of alkali, alkali earth metals and major ash forming elements during gasification of fuel cane bagasse. *Fuel* 91 (1), 253–263.
- Kantola, I.B., Masters, M.D., Beerling, D.J., Long, S.P., DeLucia, E.H., 2017. Potential of global croplands and bioenergy crops for climate change mitigation through deployment for enhanced weathering. *Biol. Lett.* 13 (4).
- Kanzaki, Y., Planavsky, N.J., Reinhard, C.T., 2023. New estimates of the storage permanence and ocean co-benefits of enhanced rock weathering. *PNAS Nexus* 2 (4), 1–9.
- Kelland, M.E., Wade, P.W., Lewis, A.L., Taylor, L.L., Sarkar, B., Andrews, M.G., Lomas, M.R., Cotton, T.E.A., Kemp, S.J., James, R.H., Pearce, C.R., Hartley, S.E., Hodson, M.E., Leake, J.R., Banwart, S.A., Beerling, D.J., 2020. Increased yield and CO₂ sequestration potential with the C4 cereal Sorghum bicolor cultivated in basaltic rock dust-amended agricultural soil. *Global Change Biol.* 26 (6), 3658–3676.
- Khalil, M.J., Aslam, M., Ahmad, S., 2021. Utilization of sugarcane bagasse ash as cement replacement for the production of sustainable concrete – a review. *Construct. Build. Mater.* 270 (2021), 121371 <https://doi.org/10.1016/j.conbuildmat.2020.121371>.
- Kingston, G., 1999. A role for silicon, nitrogen and reduced bulk density in yield responses to sugar mill ash and filter mud/ash mixtures. *Proc. Aust. Soc. Sugar Cane Technol.* 21, 114–121.
- Kristl, M., Muršec, M., Šústář, V., Kristl, J., 2016. Application of thermogravimetric analysis for the evaluation of organic and inorganic carbon contents in agricultural soils. *J. Therm. Anal. Calorim.* 123 (3), 2139–2147.
- Larkin, C.S., Andrews, M.G., Pearce, C.R., Yeong, K.L., Beerling, D.J., Bellamy, J., Benedict, S., Freckleton, R.P., Goring-Harford, H., Sadekar, S., James, R.H., 2022. Quantification of CO₂ removal in a large-scale enhanced weathering field trial on an oil palm plantation in Sabah, Malaysia. *Frontiers in Climate* 4, 959229. <https://doi.org/10.3389/fclim.2022.959229>.
- Larsen, P., Patane, P.A., Asamoah, I., 2017. Benchmarking cane supply quality in the Herbert, Burdekin, Proserpine and Plane Creek regions. *Proc. Aust. Soc. Sugar Cane Technol.* 44, 27–36.
- Larsen, P., Atkinson, C., Stringer, J., 2023. Use of mill by-products in the fallow in sugarcane production in Australia. *Proc. Aust. Soc. Sugar Cane Technol.* 39, 77–88.
- Lefebvre, D., Goglio, P., Williams, A., Manning, D.A.C., de Azevedo, A.C., Bergmann, M., Meersmans, J., Smith, P., 2019. Assessing the potential of soil carbonation and enhanced weathering through Life Cycle Assessment: a case study for São Paulo State, Brazil. *J. Clean. Prod.* 233, 468–481.
- Lewis, A.L., Sarkar, B., Wade, P., Kemp, S.J., Hodson, M.E., Taylor, L.L., Yeong, K.L., Davies, K., Nelson, P.N., Bird, M.I., Masters, M.D., DeLucia, E., Leake, J.R., Banwart, S.A., Beerling, D.J., 2021. Effects of mineralogy, chemistry and physical properties of basalts on carbon capture potential and plant-nutrient element release via enhanced weathering. *Appl. Geochem.* 132.
- Luo, Y., Zhou, X., 2006. *Soil Respiration and the Environment*. Elsevier Academic Press, Amsterdam.
- Marchuk, A., Marchuk, S., Salter, B., Panitz, J.H., Schroeder, B.L., 2018. Effect of mill mud and gypsum amendments and their combination on physicochemical properties and hydraulic conductivity of marginal soils. *Proc. Aust. Soc. Sugar Cane Technol.* 40, 97–103.
- Mitchell, R.D.J., Larsen, P.J., 2000. A simple method for estimating the return of nutrients in sugarcane trash. *Proc. Aust. Soc. Sugar Cane Technol.* 22, 212–216.
- Mitchell, R.D.J., Thorburn, P.J., Larsen, P., 2000. Quantifying the loss of nutrients from the immediate area when sugarcane residues are burnt. *Proc. Aust. Soc. Sugar Cane Technol.* 22, 206–211.
- Moody, P., Schroeder, B.L., Pu, G., Panitz, J., 2014. Effects of the application of mill mud/mud ash on soil properties and available soil nitrogen and phosphorus. *Proc. Aust. Soc. Sugar Cane Technol.* 36, 45–52.
- Negrão, D.R., Driemeier, C., 2022. Fate of silica phytoliths in the industrial crushing of sugarcane stalks. *Ind. Crops Prod.* 185 (2022), 115132.
- Nan, W., Yue, S., Li, S., Huang, H., Shen, Y., 2016. The factors related to carbon dioxide effluxes and production in the soil profiles of rain-fed maize fields. *Agric. Ecosyst. Environ.* 216, 177–187.
- Nguyen, D.H., Biala, J., Grace, P.R., Scheer, C., Rowlings, D.W., 2014. Greenhouse gas emissions from sub-tropical agricultural soils after addition of organic by-products. *SpringerPlus* 3 (1), 1–14.
- Obersteiner, M., Bednar, J., Wagner, F., Gasser, T., Caias, P., Forsell, N., Frank, S., Havlik, P., Valin, H., Janssens, I.A., Peñuelas, J., Schmidt-Traub, G., 2018. How to spend a dwindling greenhouse gas budget. *Nat. Clim. Change* 8 (1), 7–10.
- Palandri, J.L., Kharaka, Y.K., 2004. A Compilation of Rate Parameters of Water-Mineral Interaction Kinetics for Application to Geochemical Modeling.
- Parkhurst, D.L., Appelo, C.A.J., 2013. Description of input and examples for PHREEQC version 3—A computer program for speciation, batch-reaction, one-dimensional transport, and inverse geochemical calculations. In: U.S. Geological Survey Techniques and Methods, Book 6, Chapter A43, pp. 327–333. <https://pubs.usgs.gov/tm/06/a43/>.

- Parkhurst, D.L., Appelo, C.A.J., 2013. PHREEQC (Version 3).
- Patane, P., Landers, G., Thompson, M., Nothard, B., Norris, C.A., Olayemi, M., 2019. Adoption of practices to mitigate harvest losses: 2017 results. Proc. Aust. Soc. Sugar Cane Technol. 41, 488–496.
- Pogge von Strandmann, P.A.E., Tooley, C., Mulders, J.J.P.A., Renforth, P., 2022. The dissolution of olivine added to soil at 4°C: implications for enhanced weathering in cold regions. *Frontiers in Climate* 4.
- Prado, R., Caione, G., Campos, C., 2013. Filter cake and vinasse as fertilizers contributing to conservation agriculture. *Appl. Environ. Soil Sci.* 2013, 581984. <https://doi.org/10.1155/2013/581984>.
- Pratt, C., Kingston, K., Laycock, B., Levett, I., Pratt, S., 2020. Geo-agriculture: reviewing opportunities through which the geosphere can help address emerging crop production challenges. *Agronomy* 10 (7), 971.
- Queensland Department of Environment and Science, 2022. Reef Protection Regulations Farming in Reef Catchments: Prescribed Methodology for Sugarcane Cultivation.
- R Core Team, 2023. R: A Language and Environment for Statistical Computing. R Foundation for Statistical Computing, Vienna, Austria.
- Rastogi, M., Singh, S., Pathak, H., 2002. Emission of carbon dioxide from soil. *Curr. Sci.* 82 (5), 510–517.
- Renforth, P., 2012. The potential of enhanced weathering in the UK. *Int. J. Greenh. Gas Control* 10, 229–243.
- Renforth, P., Henderson, G.M., 2017. Assessing ocean alkalinity for carbon sequestration. *Rev. Geophys.* 55 (3), 636–674.
- Renforth, P., 2019. The negative emission potential of alkaline materials. *Nat. Commun.* 10 (1401) <https://doi.org/10.1038/s41467-019-09475-5>.
- Rinder, T., von Hagke, C., 2021. The influence of particle size on the potential of enhanced basalt weathering for carbon dioxide removal - insights from a regional assessment. *J. Clean. Prod.* 315, 128178.
- Saltelli, A., Annoni, P., 2010. How to avoid a perfunctory sensitivity analysis. *Environ. Model. Software* 25 (12), 1508–1517.
- Schuing, R.D., Krijgsman, P., 2006. Enhanced weathering: an effective and cheap tool to sequester CO₂. *Climatic Change* 74 (1), 349–354. <https://doi.org/10.1007/s10584-005-3485-y>.
- Smith, P., Davis, S.J., Creutzig, F., Fuss, S., Minx, J., Gabrielle, B., Kato, E., Jackson, R.B., Cowie, A., Kriegler, E., Van Vuuren, D.P., Rogelj, J., Ciais, P., Milne, J., Canadell, J. G., McCollum, D., Peters, G., Anew, R., Krey, V., Shrestha, G., Friedlingstein, P., Gasser, T., Grübler, A., Heidug, W.K., Jonas, M., Jones, C.D., Kraxner, F., Littleton, E., Lowe, J., Moreira, J.R., Nakicenovic, N., Obersteiner, M., Patwardhan, A., Rogner, M., Rubin, E., Sharifi, A., Torvanger, A., Yamagata, Y., Edmonds, J., Yongsung, C., 2016a. Biophysical and Economic Limits to Negative CO₂ Emissions. Nature Publishing Group, London, pp. 42–50.
- Smith, P., Haszeldine, R.S., Smith, S.M., 2016b. Preliminary assessment of the potential for, and limitations to, terrestrial negative emission technologies in the UK. *Environmental Science - Processes & Impacts* 18 (11), 14–145.
- Soltani, N., Bahrami, A., Pech-Canul, M.I., González, L.A., 2015. Review on the physicochemical treatments of rice husk for production of advanced materials. *Chem. Eng. J.* 264, 899–935.
- Stirling, G., Young, A.J., Aitken, R.L., Beattie, R.N., Munro, A., 2018. Effects of compost and mill/ash on soil carbon and the nematode community in a field trial on sugarcane at Harwood, New South Wales. *Proc. Aust. Soc. Sugar Cane Technol.* 40, 41–49.
- Swoboda, P., Döring, T.F., Hamer, M., 2022. Remineralizing soils? The agricultural usage of silicate rock powders: a review. *Sci. Total Environ.* 807 (Pt 3), 150976.
- Taylor, L.L., Beerling, D.J., Quegan, S., Banwart, S.A., 2017. Simulating carbon capture by enhanced weathering with croplands: an overview of key processes highlighting areas of future model development. *Biol. Lett.* 13 (4).
- Taylor, L.L., Driscoll, C.T., Groffman, P.M., Rau, G.H., Blum, J.D., Beerling, D.J., 2021. Increased carbon capture by a silicate-treated forested watershed affected by acid deposition. *Biogeosciences* 18 (1), 169–188.
- van Straaten, P., 2006. Farming with rocks and minerals: challenges and opportunities. *Anais da Academia Brasileira de Ciências (Annals of the Brazilian Academy of Sciences)* 78 (4), 731–747.
- Vassilev, S.V., Baxter, D., Andersen, L.K., Vassileva, C.G., 2013. An overview of the composition and application of biomass ash. Part 1. Phase–mineral and chemical composition and classification. *Fuel* 105, 40–76.
- Vienne, A., Poblador, S., Portillo-Estrada, M., Hartmann, J., Ijehon, S., Wade, P., Vicca, S., 2022. Enhanced weathering using basalt rock powder: carbon sequestration, co-benefits and risks in a mesocosm study with *Solanum tuberosum*. *Frontiers in Climate* 4.
- Wang, X., Tang, C., Mahony, S., Baldock, J.A., Butterly, C.R., 2014. Factors affecting the measurement of soil pH buffer capacity: approaches to optimize the methods. *Eur. J. Soil Sci.* 66, 53–64.
- Wickham, H., 2016. *ggplot2: Elegant Graphics for Data Analysis*. New York.
- Zamanian, K., Pustovoytov, K., Kuzyakov, Y., 2016. Pedogenic carbonates: forms and formation processes. *Earth Sci. Rev.* 157, 1–17.
- Zhang, G., Kang, J., Wang, T., Zhu, C., 2018. Review and outlook for agromineral research in agriculture and climate mitigation. *Soil Res.* 56 (2), 113.